#2332    THE INSTITUTE OF PAPER CHEMISTRY
(Rheology of Papermaking Materials)
Project Reports (1)

THE RHEOLOGY OF PAPERMAKING MATERIALS

A LITERATURE SURVEY*

· PART II

SURVEY AND EXPERIMENTS ON THE VIBRATING REED TECHNIQUE

*Literature survey was completed January 1, 1963

## TABLE OF CONTENTS

## INTRODUCTION

For the past few years the double electromagnetic transducer (1, 2, 3) has been used in this laboratory to determine the complex shear modulus of pads composed of wet pulp fibers. This instrument, unfortunately, is limited to shear moduli less than $5 \times 10^9$ dyne/cm.$^2$ and is not suitable for examining the time dependent properties of paper. We have, therefore, been looking for experimental techniques for obtaining the complex modulus of materials with moduli in the $10^{10}$ to $10^{12}$ dyne/cm.$^2$ range and in the 20 to 1000 c.p.s. frequency range.

In the course of our survey on the rheological properties of papermaking materials we examined a number of experimental techniques suitable for examining the time dependent mechanical properties of paper. One of these techniques, the vibrating reed technique, appeared to be promising enough to warrant experimental investigation under the present project. The present report contains the results of some of our investigations on paper and Mylar film.

## THE VIBRATING REED METHOD

In the vibrating reed method the clamped end of a cantilever beam is caused to oscillate with a sinusoidal frequency. The displacement of the free end of the beam is observed as a function of frequency. The resonant frequency and band width are determined from amplitude-frequency curves and used to calculate the real and imaginary components of the complex Young's modulus.

If the transverse dimension of the viscoelastic beam is small compared to both its length and the accoustical wavelength, the fundamental equation of motion is given by (4),

$$A\rho \frac{\partial^2 y}{\partial t^2} + E'I \frac{\partial^4 y}{\partial x^4} + \eta'I \frac{\partial^5 y}{\partial x^4 \partial t} = 0. \tag{1}$$

Here, $x$ denotes the distance along the reed measured from its clamped end and $y$ is the displacement normal to it. Also, $t$ is the time, $I$ is the moment of inertia of the cross-sectional area $A$ about its neutral axis, $\rho$ is the density of the material, $E'$ is the real component of the complex Young's modulus and $\eta'$ is the dynamic viscosity coefficient.

The problem of the vibrating reed has been considered by a number of authors. Nolle (5) obtained solutions to the vibrating reed problem by considering the solution of an equivalent electrical network. A more rigorous analysis of the problem is given by Horio and Onogi (4). This method assumes a simple form for the variation of the complex modulus across the width of the resonance curve and is valid as long as the mechanical loss tangent is less than $10^{-1}$. For those materials where the frequency dependence of the modulus has a profound effect on the frequency and amplitude of the resonance peak, the analysis of Bland and Lee (6) must be considered.

According to Horio and Onogi (4) the complex Young's modulus is given by,

$$E^* = E' + j E'' \tag{2}$$

where $j = \sqrt{-1}$ and $E'$, the real component of the modulus, is given by,

$$E' = (\rho A / a_o^4 I) \ell^4 [\omega_o^2 + \frac{1}{8}(\Delta\omega)^2] \tag{3}$$

and $\underline{E}''$, the imaginary component, is,

$$E'' = (\rho A/a_o^4 I)\ell^4 \,\Delta\omega\,\omega_o. \tag{4}$$

The circular frequency $\omega_o$ is the resonance frequency at which the amplitude of the free end of the reed is a maximum and the band width $\Delta\omega$ is the difference in frequencies at which the amplitude is $1/\sqrt{2}$ times its maximum value. Also, $\ell$ is the length of the reed and $\underline{a}_o = 1.875,\ 4.694,\ 7.855$ for the fundamental mode, first harmonic, and second harmonic of vibration, respectively.

For paper ($\underline{7}$), 6,6-nylon ($\underline{8}$), viscose rayon ($\underline{8},\ \underline{9}$), acetate rayon ($\underline{8},\ \underline{9}$), and silk ($\underline{9}$), $E''$ is independent of frequency and Meredith and Hsu ($\underline{8}$) have shown that Equations (3) and (4) can be written as:

$$E' = ((\rho A/a_o^4 I)\ell^4 \omega_o^2 \tag{5}$$

and

$$E'' = (\rho A/a_o^4 I)\ell^4 \omega_o \Delta\omega[1 + (1/8)(\Delta\omega/\omega_o)]. \tag{6}$$

The mechanical loss tangent $\tan\Delta$ is given by,

$$\tan\Delta = (\Delta\omega/\omega_o)[1 + (1/8)(\Delta\omega/\omega_o)^2]. \tag{7}$$

When $\Delta\omega/\omega_o$ is less than 0.2, the second power term in the bracket can be ignored with an error of less than one-half per cent. For these special materials the resonance frequency is independent of internal damping and is equal to the natural frequency of the purely elastic system.

The equations given thus far are valid only under conditions where
air damping is unimportant or where appropriate corrections have been made.
In the present work air damping corrections were found to be important and
will be discussed in detail in the experimental section of this report.

### GENERAL EXPERIMENTAL PROCEDURES AND TECHNIQUES

#### THE VIBRATING REED APPARATUS

The basic unit of the vibrating reed apparatus is an Astatic (10)
type M 41-8 magnetic recording head of the type used in the cutting of
phonograph records as shown in Figure 1. The recording needle has been
replaced by a lightweight clamp consisting of a Cook's (11) No. 2 file-
signal silver soldered to 5/8 by 0.037-inch diameter stainless steel pin.
The weight of the clamp is approximately 0.6 gram. The resonance frequency
of the unloaded clamp when mounted in the recording head is above 1000 c.p.s.
for a typical clamp assembly.

The signal from a Hewlett-Packard model 200 J audio oscillator (12)
is amplified by means of a McIntosh Model MC-30, 30-watt power amplifier
(13) and then supplied to the recording head. The recording head is mounted
in a 6-3/4 by 3-inch diameter vacuum chamber having a 1/2-inch thick Lucite
window at one end through which the amplitude of the vibrating reed can be
observed by means of a traveling microscope.

#### SUITABLE EXPERIMENTAL MATERIALS

In general any flat paper stock or board up to 0.020-inch thick is
suitable for vibrating reed measurements. The only requirement is that the
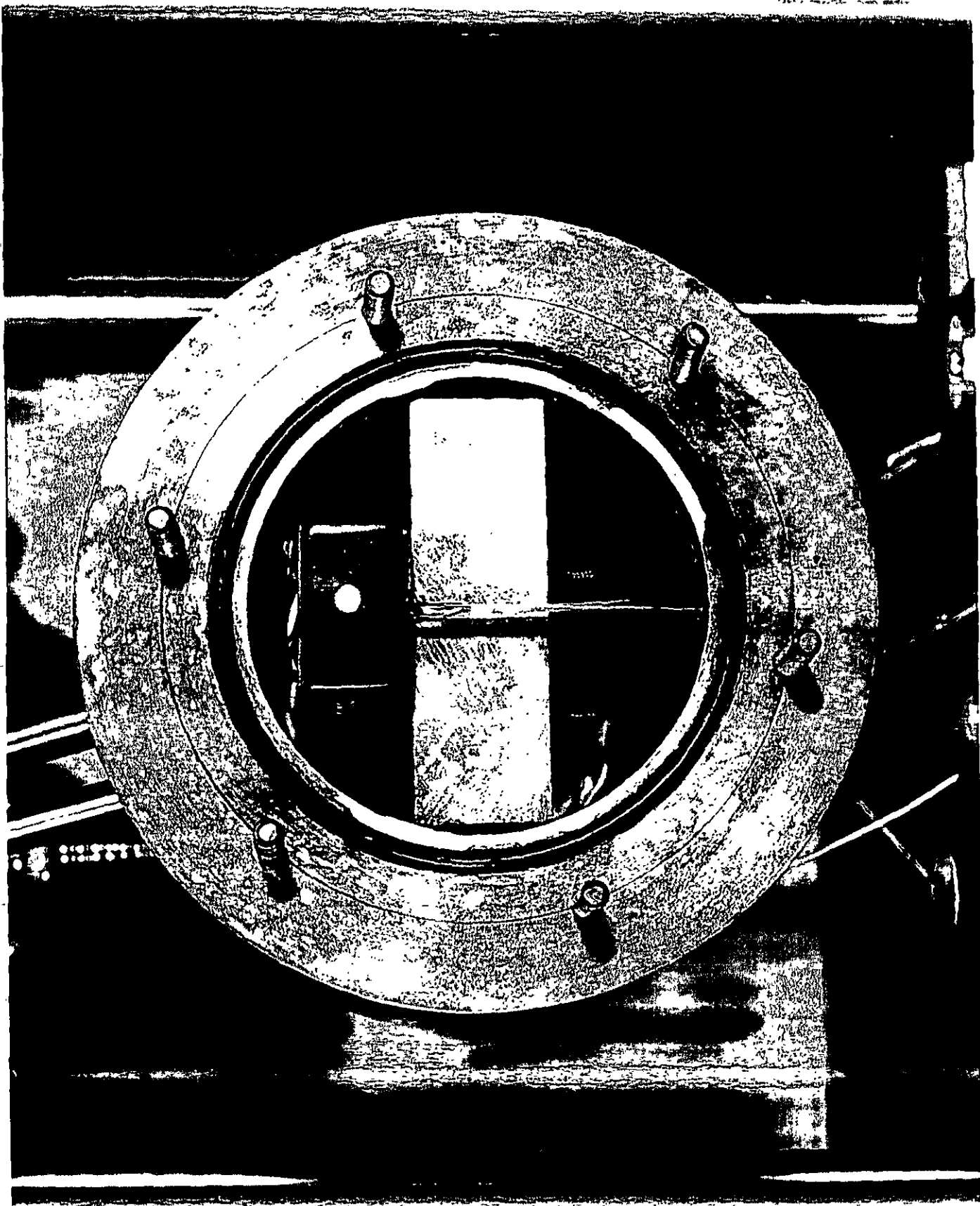the material be cut to a reed approximately 1 cm. wide and 4 to 5 cm. long.

Figure 1. Photograph of Vacuum Chamber Recording Head and Reed Used in Vibrating Reed

Crystalline polymeric films are also suitable as are metal foils and coated papers.

Rubberlike polymeric films are, in general, unsuitable unless they are examined at temperatures below their glass transition temperatures. Above the glass temperature they absorb too much energy and cannot be set into a resonance that can be observed since the accoustic wave is damped out by the time it reaches the end of the reed.

EXPERIMENTAL PROBLEMS

There are a number of problems that arise in obtaining reliable experimental data and it is profitable to consider them at this point in our discussion.

The primary experimental measurements involve the determination of the amplitude of vibration as a function of frequency. Typical plots resulting from such measurements are shown in Figure 2 for Mylar film and a sample of southern softwood solid fiberboard milk carton stock in vacuum. In the case of the milk carton stock the vacuum was maintained 24 hours before the measurements were taken.

The curves are of interest since they represent data taken on reeds of comparable length and have resonance frequencies that are similar. The original amplitude data have been adjusted so that the curves for both samples have a maximum amplitude of 0.05 cm. at resonance.

Several features are noteworthy. First, the resonance peaks are not symmetrical about the resonance frequency. This behavior is typical of this type of experiment and, indeed, is predicted by theory (4). Secondly,
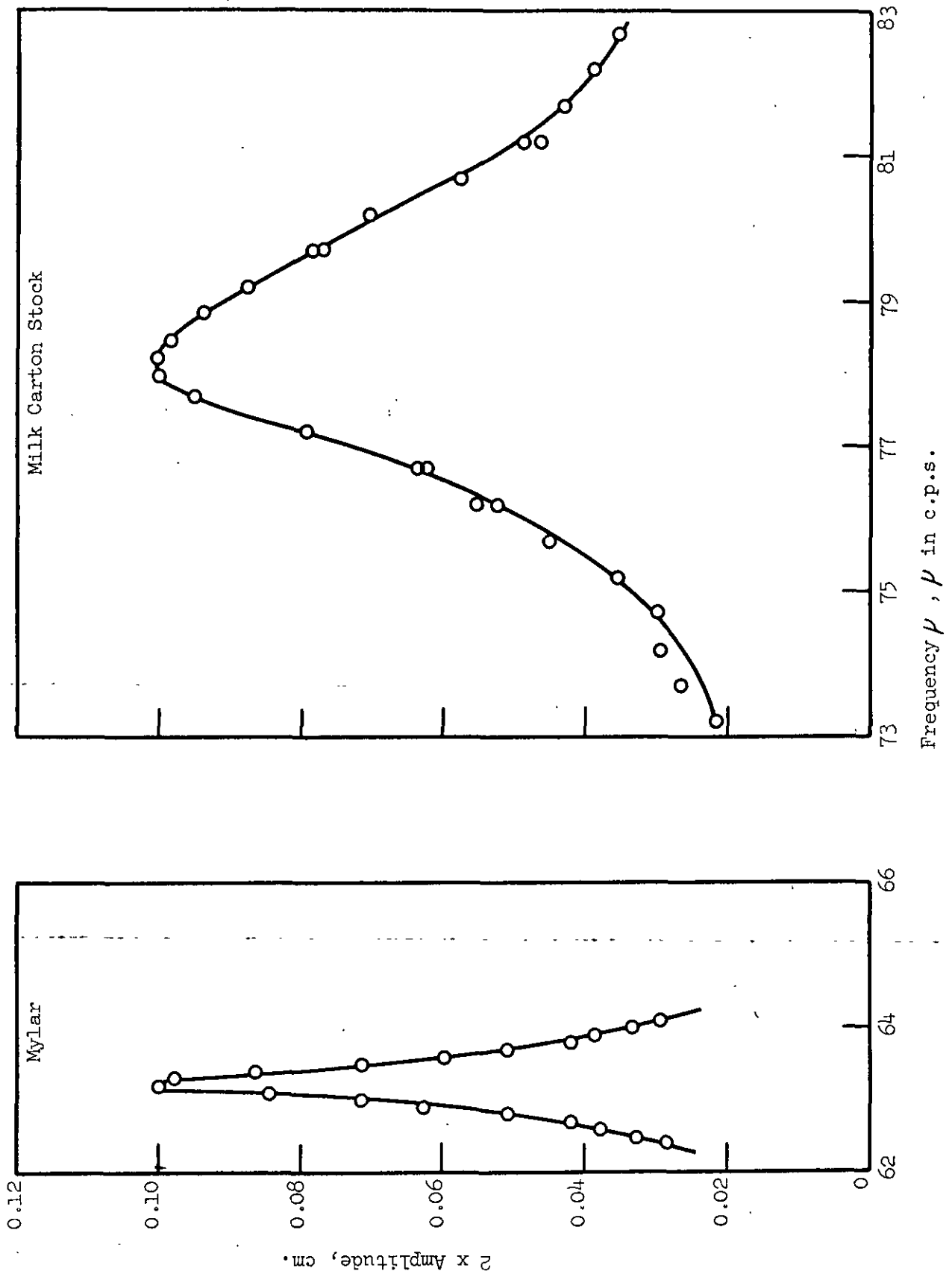
Figure 2. Amplitude-Frequency Curves for Mylar Film and Paper

the band width, $\Delta\omega$, of the two materials is considerably different. This reflects differences between the mechanical loss tangents of the two materials. The mechanical loss tangent, Equation (7), can be written as,

$$\tan\Delta = \Delta\omega/\omega_0$$

$$\propto \frac{(\text{energy lost/cylce})}{(\text{energy stored/cycle})} \; . \quad\quad (8)$$

The mechanical loss tangent, therefore, is proportional to the ratio of the energy lost to the energy stored in taking the reed through a cyclic deformation and is a measure of sample deadness.

From the curves in Figure 2 the mechanical loss tangent for Mylar was $\tan\Delta = 0.0081$ and for the milk carton stock, $\tan\Delta = 0.042$. This difference in energy dissipation for the two materials causes a significant difference between the two as far as sensitivity to room vibration is concerned. With a 0.0206 by 0.4717 by 4.351-cm. Mylar reed, normal laboratory vibrations such as a person walking in the room, are great enough to make measurement impossible unless special precautions are taken to eliminate vibration. In order to obtain the Mylar data of Figure 2, it was necessary to mount the instrument on rubber chock mountings and to work evenings or during laboratory quiet hours. In the case of paper, no particular difficulty was encountered since the mechanical loss is great enough to damp out room vibrations.

AIR DAMPING

Air damping affects both the resonance frequency and the band width of the vibrating reed so that if Equations (5), (6), and (7) are to be used appropriate corrections must be made or the air damping must be eliminated. The simplest procedure is to evacuate the sample chamber and thereby eliminate the source of air damping. This is suitable for polymeric materials such as Mylar where one is not in danger of altering the mechanical properties of the reed by evacuation.

In order to illustrate the effect of air damping we have shown typical amplitude-frequency curves for a 3.88 by 0.0447 by 0.95-cm. reed of southern softwood solid fiberboard milk carton stock in Figure 3. All curves were obtained using the same driving voltage on the recording head.

The reed was held under a vacuum of 56 mm. Hg. for 24 hours and the amplitude-frequency curve was obtained with a maximum amplitude of 0.0615 cm. at a resonance frequency of 78.1 c.p.s. and a band width of 3.2 c.p.s. Dry air, obtained by passing air through a drierite column, was admitted to the vacuum chamber. The resonance frequency at atmospheric pressure decreased to 76.1 c.p.s., and the maximum amplitude at resonance decreased to 0.0525 cm. The band width increased to 3.25 c.p.s. as a result of air damping. The reed was then conditioned for 24 hours at 50% R.H. and the resonance frequency decreased to 72.7 c.p.s. and the band width increased to 3.5 c.p.s.

It is apparent that for paper simple evacuation of the chamber to reduce air damping is not satisfactory since in addition to eliminating air damping, the moisture content of the paper is altered and hence, the
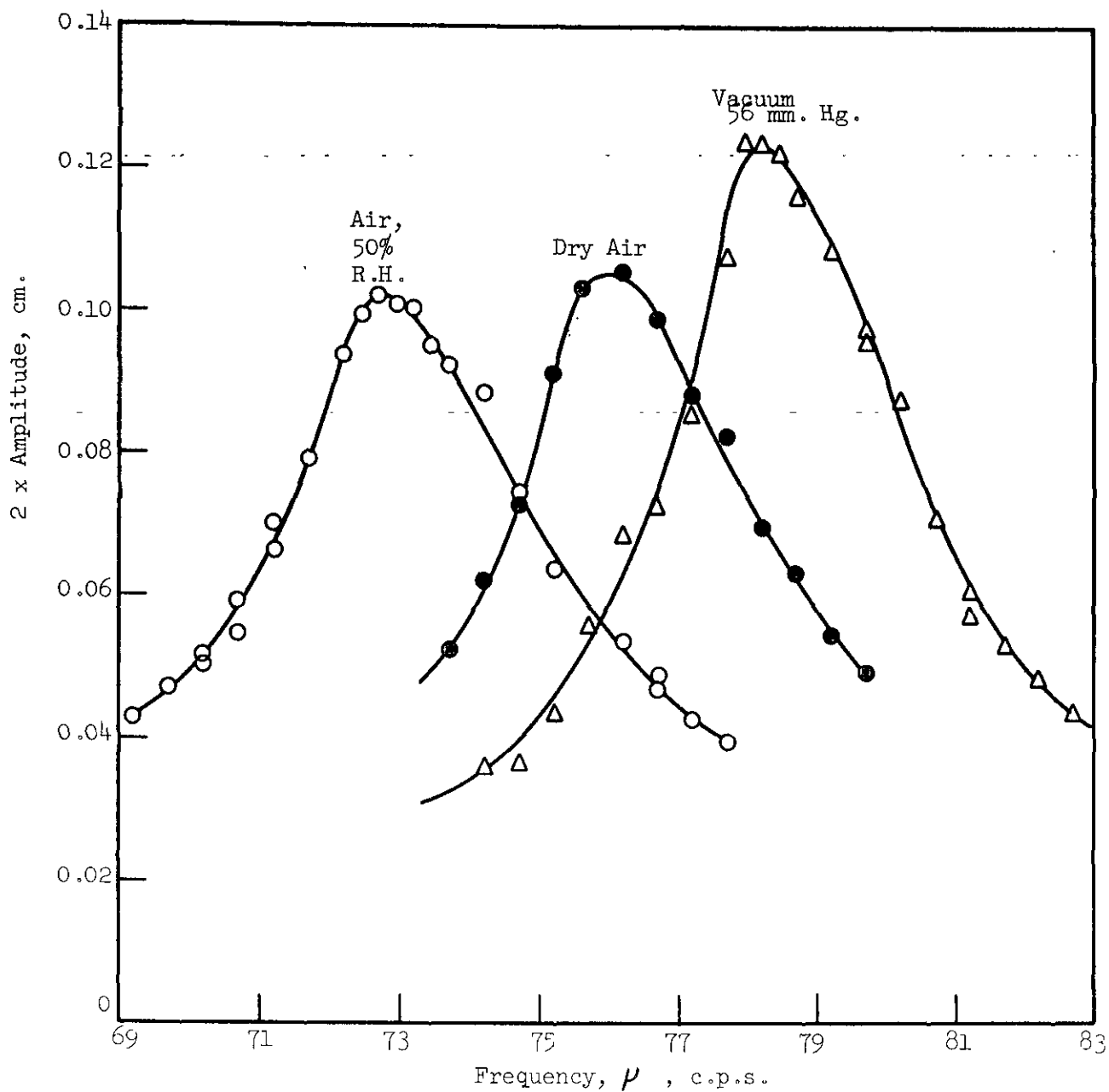
Figure 3. The Effect of Air and Vacuum on the Amplitude-Frequency Curves
for a Sample of Southern Softwood Solid Fiber Board Milk
Carton Stock

mechanical properties. For paper, therefore, it is necessary to resort to theoretical corrections for air damping.

Several investigators (14, 15, 8) have considered the effect of air damping on a vibrating reed. The treatments are based on an equation due to Stokes for the resistance per unit length experienced by a rigid pendulum consisting of a cylinder oscillating in an infinite mass of viscous fluid. The frictional resistance $\varsigma$ per unit length is given by,

$$\varsigma = -k\rho_a A\frac{\partial^2 y}{\partial t^2} - k'\rho_a A\omega\frac{\partial y}{\partial t} \tag{9}$$

where $\rho_a$ is the density of air and $A$ is the cross-sectional area of the cylinder. The first term in the equation represents the effect of the inertia of the displaced fluid and affects the frequency of oscillation. The second term is the viscous damping which will diminish the amplitude as well as the frequency of oscillation. The terms $k$ and $k'$ are complicated functions of the dimensionless parameter $m$ defined by $m^2 = \rho_a A/4\pi\mu$ where $\mu$ is the viscosity of the fluid.

When Equation (1) is written to take into account the frictional resistance of the air, the band width becomes,

$$\Delta\omega = \Delta\omega_a[1 - (1/4)(\Delta\omega_a/\omega_a) + (3/32)(\Delta\omega_a/\omega_a)^4](1 + \beta k) - \beta k'\omega_a \tag{10}$$

where $\Delta\omega_a$ is the band width in air. The resonance frequency of the undamped system is given by,

$$\omega_o = \omega_a[1 + (1/4)(\Delta\omega_a/\omega_a)^2 - (5/32)(\Delta\omega_a/\omega_a)^4](1 + \beta k/2) \tag{11}$$

where $\omega_a$ is the resonance frequency in air. The quantity $\beta$ is given by $\beta = \rho_a/\rho$ where $\rho_a$ is the density of air and $\rho$ the density of the material in the reed.

## EXPERIMENTS ON MYLAR FILM

The first phases of our experimental program involved vibrating reed experiments on a sample of Du Pont Mylar Film (polyethylene terephthalate). The film was 0.0206 cm. thick and had a density of 1.380 g./cm.$^3$.

A 0.4717 by 4.351-cm. reed was cut with a razor blade and straight edge from a larger Mylar sheet. The thickness of the reed was determined with a micrometer caliper and the width and effective length of the reed were determined by means of the traveling microscope.

All experiments were conducted in a vacuum of 60 mm.-Hg. in order to eliminate air damping. The resonance frequency is inversely proportional to the square of the reed length so that a range of frequencies may be covered by progressive reduction in reed length. By this means it was possible to conduct experiments between 32 and 680 c.p.s.

The results of the experiments on Mylar film are shown in Figure 4. The real component $\underline{E}'$ of the complex Young's modulus is essentially independent of frequency while the imaginary component increases from a value of $3.7 \times 10^8$ dyne/cm.$^2$ at 32 c.p.s. to $6 \times 10^8$ dyne/cm.$^2$ at 680 c.p.s. The frequency behavior of $\underline{E}'$, $\underline{E}''$ and $\tan\delta$ are typical of crystalline polymers.

The values of $\underline{E}'$ and $\underline{E}''$ may be determined to approximately $\pm 12\%$. This rather large error is due primarily to the fourth power dependence of the moduli on length and the dependence on the cube of the thickness. These experiments were conducted before our techniques of reed cutting were fully developed. With our present techniques as described in the following section this error can be somewhat reduced.
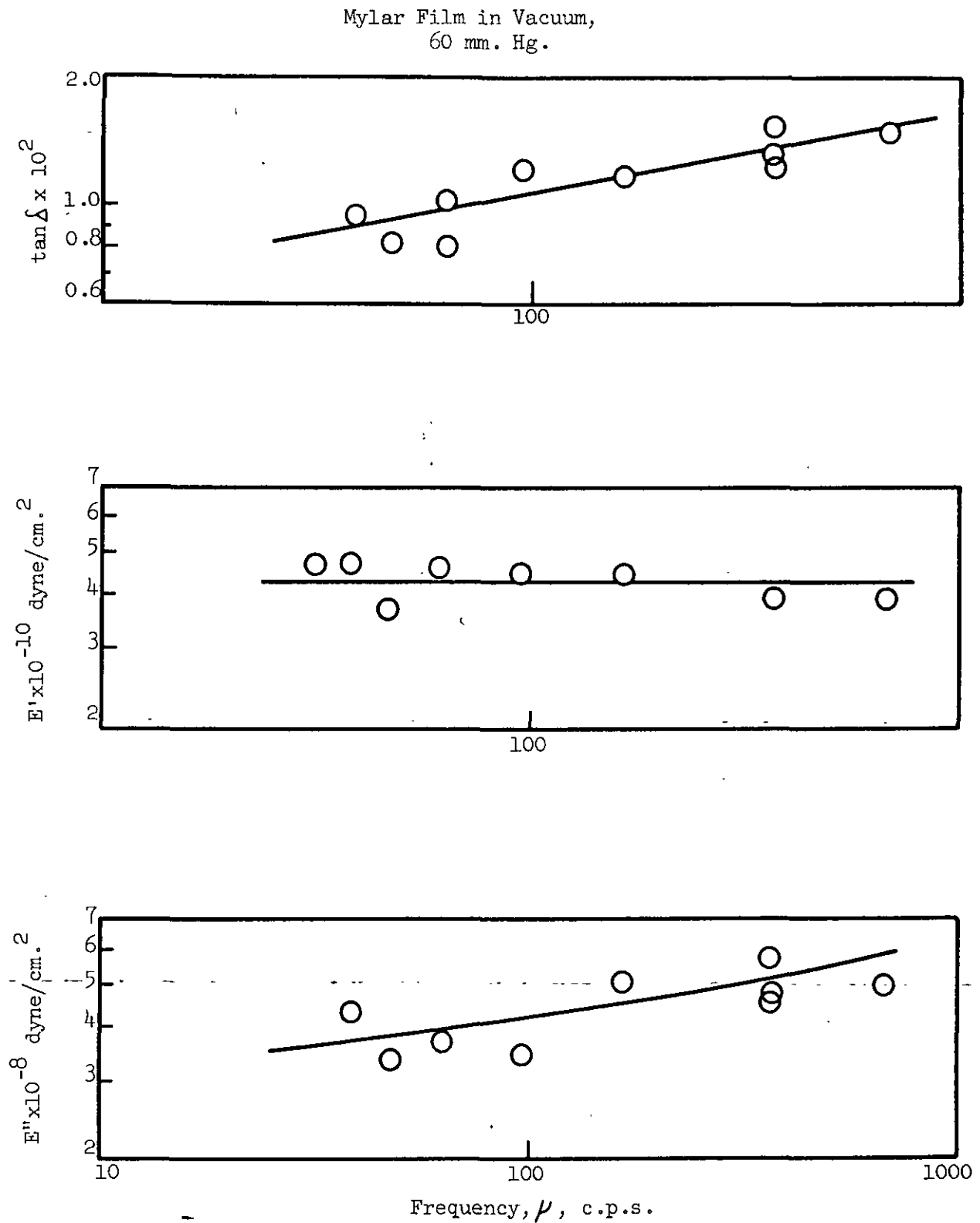
Mylar Film in Vacuum,
60 mm. Hg.



Figure 4.  Real and Imaginary Components of the Complex Young's Modulus
and Mechanical Loss Tangent for Mylar Film

EXPERIMENTS ON PAPER

MATERIALS AND SAMPLE PREPARATION

A western softwood bleached sulfite pulp was chosen for our experiments on paper. This pulp was 100% softwood, fully bleached, containing 80 to 90% spruce, 10 to 20% true fir, and a trace of cedar. The fibers showed a moderate amount of cutting and fibrillation and fines.

A series of five handsheets was prepared ranging from a basis weight of 106 g./m$^2$ to 450 g./m.$^2$ with a corresponding density range of 0.737 to 1.01 g./cc. The handsheets were prepared from the pulp on a 9 by 9-inch Valley sheet mold with a 66-inch high aluminum headbox. The headbox allowed sufficiently high dilution of the stock to give sheets of good formation. The sheets were couched from the wire with dry blotters and pressed at 700 p.s.i. in a small handpress for approximately five minutes. The sheets were then removed from the press, new blotters applied and the sheets pressed again. This procedure was repeated until the sheets were essentially dry.

The special procedure for drying sheets was necessary to produce sheets from which flat reeds could be obtained. The normal drying procedures, using British standard TAPPI drying rings or a steam chest, produce handsheets with some curvature and do not yield reeds which are sufficiently flat for vibrating reed measurements.

Reeds were cut from these pressed sheets with The Institute of Paper Chemistry precision paper cutter (16). With this cutter it was possible to cut rectangular reeds with parallel edges and square ends. The reeds were then cemented to the reed holders with Epoxy resin.

A series of brief experiments were conducted to see whether or not reeds in this basis weight range were suitable for vibrating reed experiments. The experiments were conducted under a high vacuum of 0.07 μ and in dry nitrogen at atmospheric pressure. All of the reeds were found suitable for measurement and would have required air damping corrections had we wished to calculate their complex moduli.

Rather than conduct experiments on all five basis weight reeds a single reed was selected as representative of the pulp and our experiments were confined to it. The reed had a basis weight of 215 g./m.$^2$, an apparent density of 0.8419 g./cc., and was 0.0256 cm. thick, 0.900 cm. wide, and had a free length of 3.732 cm. at 50% R.H.

## BAND WIDTH AND RESONANCE FREQUENCY; SHORT METHOD

In the experiments on Mylar film the entire amplitude-frequency curves were obtained and used to determine the band width and resonance frequency. Since this requires from 20 to 30 thirty minutes, the procedure is too time consuming for routine testing. A short method of determining the resonance frequency and band width has been devised and these quantities can now be determined in a few minutes without any sacrifice in the accuracy of the determination. This short method was used on all of our experiments on paper.

In the short method, the resonance frequency is observed by setting the cross hairs of the traveling microscope near the maximum amplitude and then adjusting the frequency to yield a maximum reed amplitude. The frequency at which the maximum amplitude is observed is the resonance frequency.

From the traveling microscope settings at maximum amplitude it is
possible to calculate one of the two microscope settings corresponding to
$1/\sqrt{2}$ times the maximum amplitude. The microscope is set at this point and
the frequency is adjusted until the reed amplitude corresponds with this
setting. This will occur at two frequencies, one on either side of the
resonance frequency. The difference between the two frequencies is the
band width.

## MOISTURE CONTENT AND DIMENSIONAL CHANGES

Moisture has several effects on the mechanical properties measured
by the vibrating reed technique. The dimensions of the reed as well as the
apparent density depend on the moisture content so that these changes must
be considered in determining the modulus. The moisture also serves as a
plasticizer and alters both real and imaginary components of the complex
modulus.

In order to keep track of the dimensional changes of the reed a
5 by 6-inch rectangular piece of stock from which the reed was cut was
conditioned along with the reed. Reference marks were placed on the strip
and changes in thickness and length were noted whenever the moisture content
of the reed and reference strip were changed. The distance between the
reference marks was measured to 0.005 inch with a steel rule and the
thickness with a Federal gage.

The reference specimen was weighed on an analytical balance
whenever the moisture content was altered. At the conclusion of a set of
experiments as a function of moisture content the reference specimen was
oven dried and the absolute moisture contents were then calculated for

each moisture condition. The relative humidity was always noted for a given moisture content.

CORRECTIONS FOR AIR DAMPING

Air damping corrections were of considerable importance and were determined from experiments conducted under high vacuum and in dry nitrogen. The vacuum chamber containing the reed was attached to the high vacuum line of the gas adsorption apparatus and held at a pressure of $0.07\ \mu$ for 24 hours. The band width and resonance frequency were then determined as a function of the amplitude of oscillation. Both were found to be amplitude dependent as a result of nonlinear viscoelastic effects. Air damping was negligible in this system since the mean free path of an air molecule is of the order of 17 cm. at this pressure.

Dry nitrogen was admitted to the chamber and the experiment was repeated as a function of amplitude. Equations (10) and (11) were then used to calculate $\underline{k}$ and $\underline{k}'$ as a function of amplitude. The value of $\rho$ was taken as $\rho = 1.40 \times 10^{-3}$. Values of $\underline{k}$ and $\underline{k}'$ were plotted as a function of reed amplitude as shown in Figure 5. Correction factors were obtained from these plots assuming that $\underline{k}$ and $\underline{k}'\omega$ are independent of frequency.

## RESULTS AND DISCUSSION

The results of vibrating reed experiments on the western softwood bleached sulfite pulp are shown in Figures 6 and 7 where the real and imaginary components of the complex Young's modulus are shown as a function of the maximum dynamic strain $\epsilon$ given by,
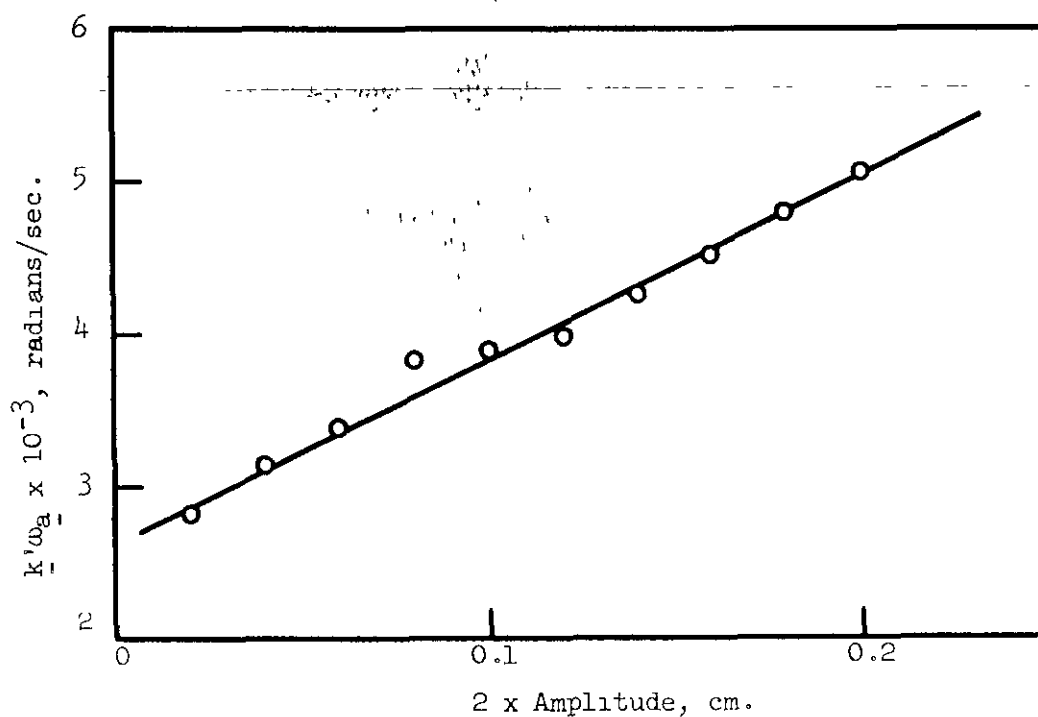
$$\epsilon = 4\ ty_m/\ell^2 \qquad\qquad (12)$$
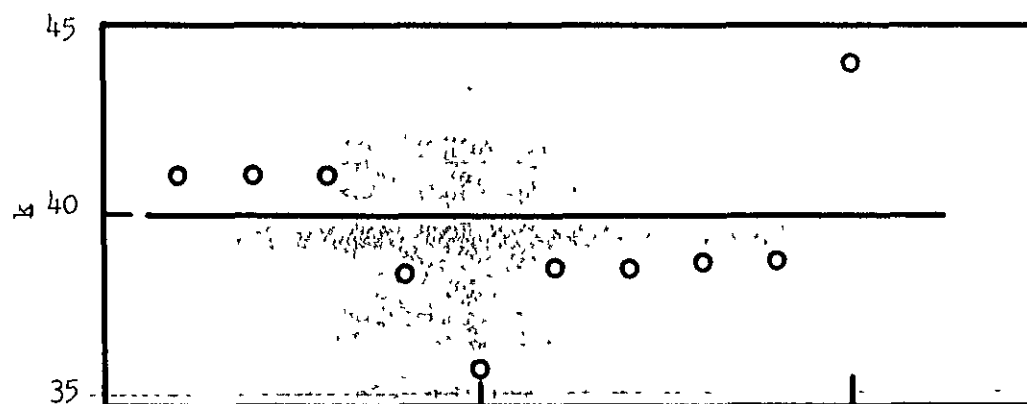
Figure 5.   Air Damping Factors k and k'ω$_a$ as a Function of
Amplitude of Vibration for a 0.0256 x 0.900 x 3.732 cm.
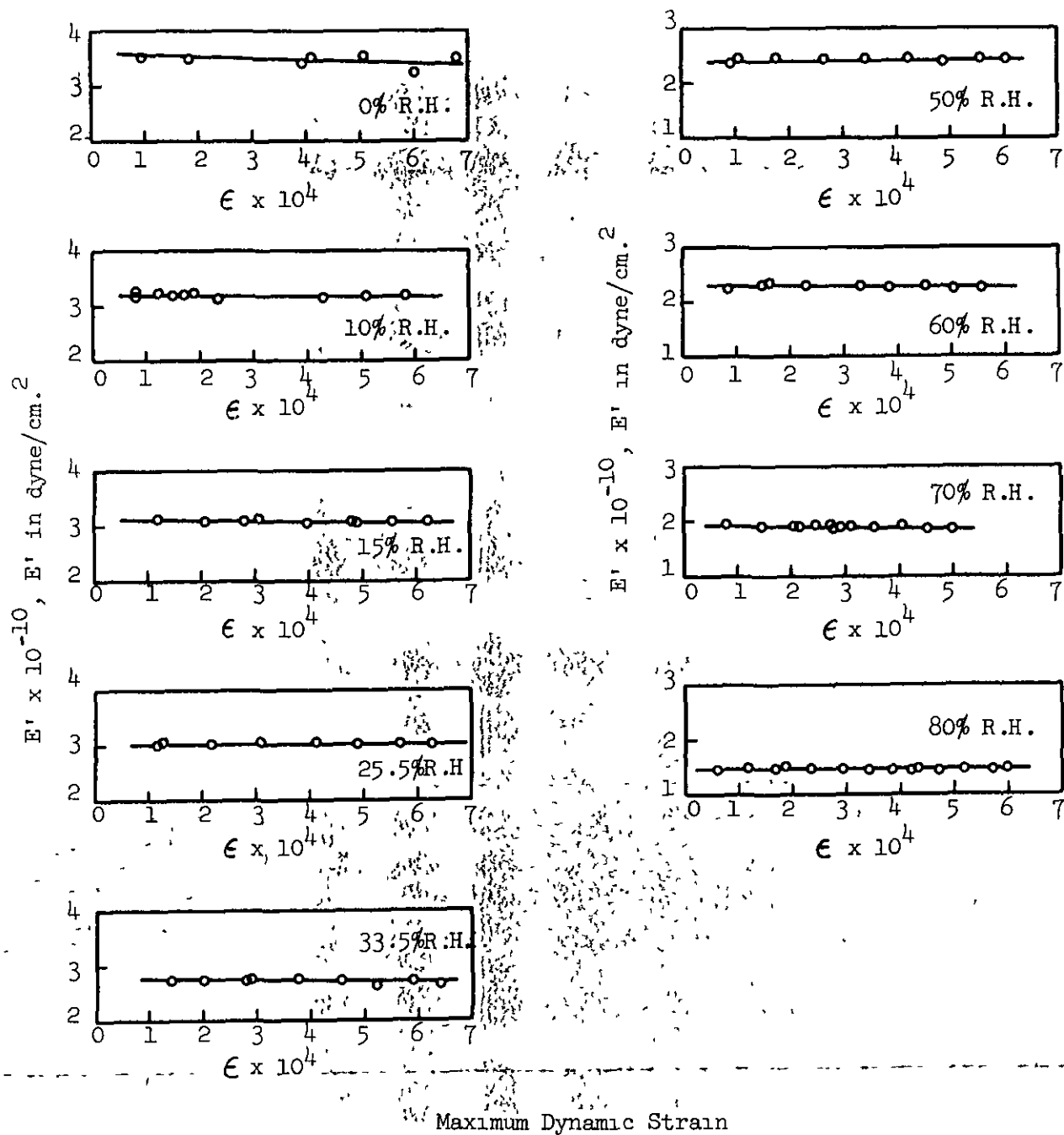Reed of Western Softwood Pulp

Figure 6. Real Component of the Complex Young's Modulus for a Western Softwood Bleached Sulfite Pulp as a Function of Maximum Dynamic Strain.
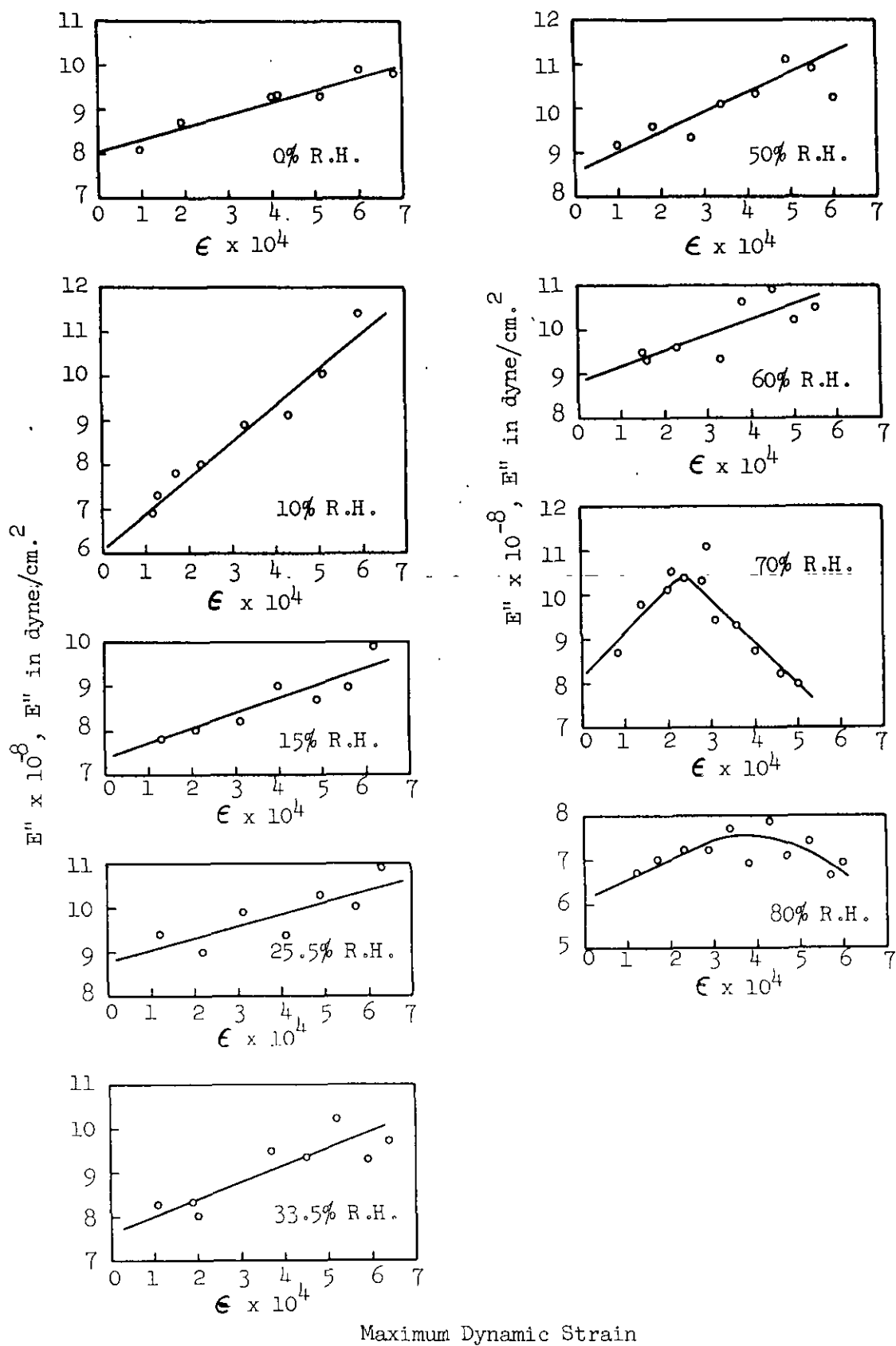
Figure 7. Imaginary Component of the Complex Young's Modulus for a
Western Softwood Bleached Sulfite Pulp as a Function of
Maximum Dynamic Strain

where $t$ is the thickness of the reed, $\ell$ is its free length, and $y_m$ is the maximum displacement of the reed. The corresponding relative humidities, moisture contents, reed dimensions, and approximate resonance frequencies and band widths are indicated in Table I. The components of the complex Young's modulus were determined at strains up to $\epsilon = 7 \times 10^{-4}$ and over a humidity range from 0 to 80% R.H.

The real component, $E'$, decreased only slightly with increasing strain. The behavior of the imaginary component is more complicated. In general, $E''$ increases with increasing dynamic strain except above 70% R.H. where a maximum is observed. This peculiar strain dependence of $E'$ and $E''$ appears to be characteristic of crystalline polymeric materials and has been observed for cotton, viscose rayon, and nylon (17). The strain behavior of the mechanical loss tangent is shown in Figure 8 and is similar to the strain behavior observed for $E''$.

The behavior of $E'$, $E''$, and $\tan\delta$ extrapolated to zero strain is shown in Figure 9 as a function of moisture content. There is a linear decrease in $E'$ with increasing moisture content and $E'$ decreases from a value of $3.60 \times 10^{10}$ dyne/cm.$^2$ at 0% moisture to $1.45 \times 10^{10}$ dyne/cm.$^2$ at 13.7% moisture. The imaginary component shows a distinct drop from a value for $E''$ of $8.05 \times 10^8$ dyne/cm.$^2$ at 0% moisture to a value of the order of $6 \times 10^8$ dyne/cm.$^2$ at 2.7% moisture. The values of $E''$ then rise to a maximum of $8.5 \times 10^8$ dyne/cm.$^2$ at 8% moisture and then decrease to $6 \times 10^8$ dyne/cm.$^2$ at 13.7% moisture.

The mechanical loss tangent is similar to $E''$ in its behavior at low moisture contents but approaches an asymptotic limit of 0.041 at high moisture contents rather than passing through a maximum at 8% moisture.

## TABLE I

SUMMARY DATA FOR A REED OF WESTERN SOFTWOOD BLEACHED SULFITE PULP

| Relative Humidity, % | Moisture, % | Length, $\ell$, cm. | Thickness, $t$, cm. | Sheet Density, $\rho$, g./cm.$^3$ | Resonance* Frequency, $\nu_o$, c.p.s. | Band* Width, $\Delta\nu$, c.p.s. |
|---|---|---|---|---|---|---|
| 0 | 0 | 3.715 | 0.02410 | 0.8618 | 57.4 | 1.3 |
| 10 | 2.76 | 3.715 | 0.02410 | 0.8618 | 54.5 | 1.1 |
| 15 | 3.56 | 3.715 | 0.02433 | 0.8605 | 54.5 | 1.3 |
| 25.5 | 4.64 | 3.718 | 0.02469 | 0.8550 | 54.8 | 1.6 |
| 33.5 | 5.69 | 3.722 | 0.02507 | 0.8494 | 52.6 | 1.6 |
| 50.0 | 7.47 | 3.729 | 0.02563 | 0.8419 | 50.8 | 1.8 |
| 60 | 8.36 | 3.732 | 0.02588 | 0.8393 | 50.1 | 1.8 |
| 70 | 10.33 | 3.732 | 0.02654 | 0.8321 | 46.9 | 1.8 |
| 80 | 13.69 | 3.744 | 0.02761 | 0.8205 | 43.1 | 1.7 |

*The values are reported at zero dynamic strain and have been corrected for air damping.
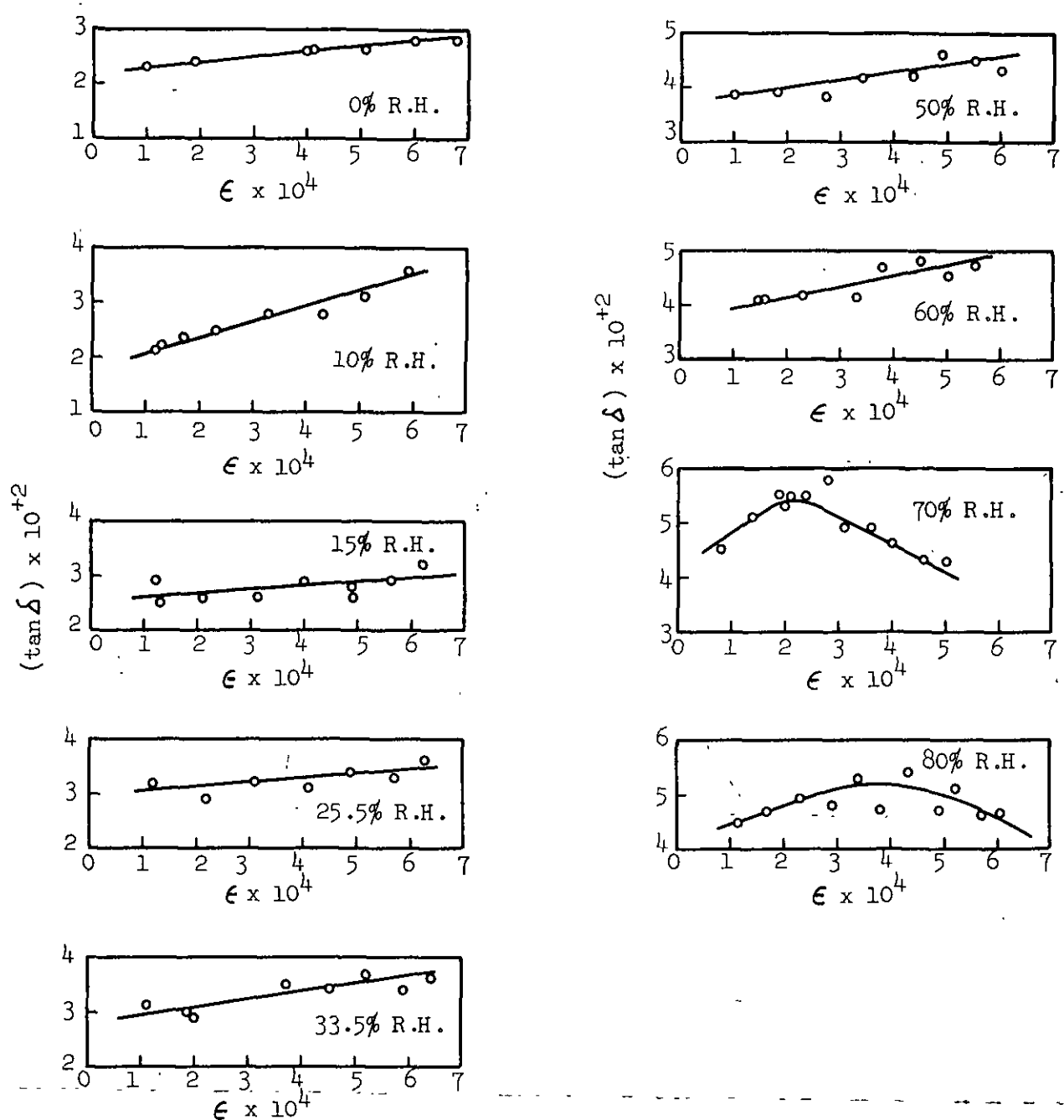
Maximum Dynamic Strain

Figure 8.   Mechanical Loss Tangent for a Western Softwood Bleached Sulfite
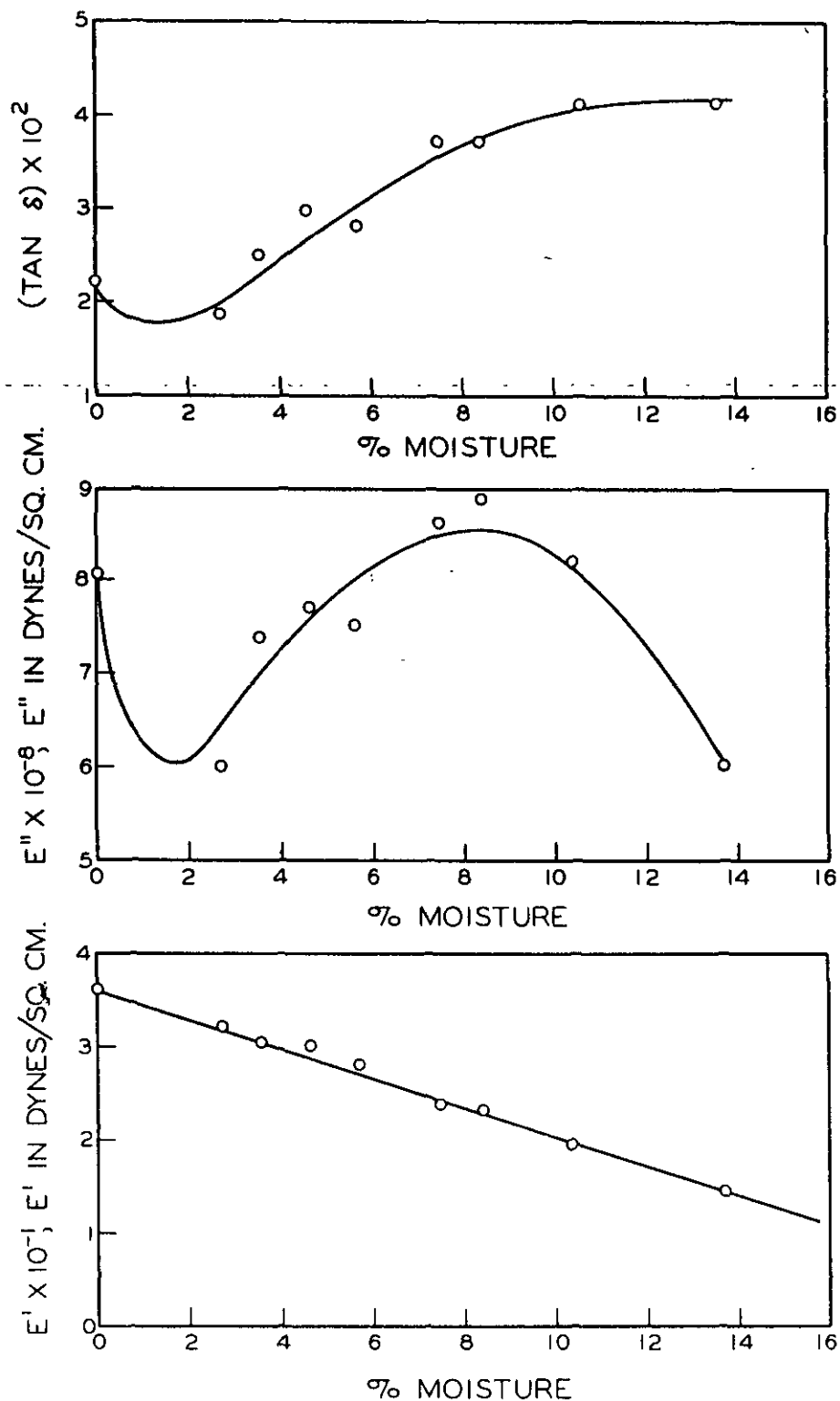Pulp as a Function of Maximum Dynamic Strain

Figure 9.  Real and Imaginary Components of the Complex Young's Modulus and
the Mechanical Loss Tangent at Zero Strain for a Western Softwood
Bleached Sulfite Pulp as a Function of Moisture Content

From the behavior of the mechanical loss tangent with increasing moisture content there appear to be two loss mechanisms. One is associated with the "dry" cellulose and the other with the plasticizing effect of the water. The source of these mechanisms is probably molecular in nature but cannot at present be attributed to a specific type of motion such as the motion of anhydroglucose units, hydroxyl group motion or relative motion between polymer molecules lying in successive crystallographic planes. The loss mechanisms do not appear to reflect changes in sheet structure since sheet geometry factors cancel out in the expressions for the loss tangent.

Above a moisture content of 8% where $E''$ passes through a maximum, the $E''$ vs. $\epsilon$ measurements are somewhat dependent on strain history. This reflects primarily a strain-history dependence of the polymeric substance of the fiber resulting from nonlinear viscoelastic effects rather than structure breakdown of the sheet. This conclusion is based on the fact that tan $\delta$ also shows a strain-history dependence and, as we have stated, this quantity is independent of sheet structure.

THE VIBRATING REED TECHNIQUE AND PULP AND PAPER CHARACTERIZATION

The vibrating reed technique shows considerable promise as a tool for the characterization of pulp and paper. The technique provides a convenient means of determining Young's modulus in flexure and is suitable for papers having a Young's modulus ranging from $0.38$ to $46 \times 10^{10}$ dyne/cm.$^2$ (7). Any uniform paper sheet is suitable provided it is thick enough to obtain reliable measurements of thickness and not too rough or soft.

By determining the real and imaginary components of the complex Young's modulus one can calculate the mechanical loss tangent. Since this quantity is independent of sheet geometry it is a useful index to changes taking place at the molecular level.

Corrections for air damping are easy to make so that the technique can be used to study the effect of moisture on the mechanical properties. In addition, by using a short reed one can conduct measurements at frequencies approaching 1,000 c.p.s. and thereby obtain the complex Young's modulus in the time scales common to calendering and corregating operations.

The cost of the experimental equipment involved is nominal and the measurements are such that they can be made by a good technician. The accuracy of the method depends to a large extent on the nature of the sheet being tested; however, an accuracy of $\pm 10\%$ for $E'$ is typical of measurements with paper. Relative changes in modulus may be obtained with greater accuracy if, for example, experiments such as we have reported are conducted as a function of humidity on a single reed. In this case relative changes in $E'$ can be determined to $\pm 2\%$ and changes in $E''$ to approximately $\pm 5\%$.

LITERATURE CITED

1. Kurath, S. F., Passaglia, E., and Pariser, R., J. App. Poly. Sci. 1:150 (1959).

2. Kurath, S. F. Construction of a double electromagnetic transducer. Progress Report One, Project 2045, The Institute of Paper Chemistry, Appleton, Wis. June 30, 1958.

3. Kurath, S. F., Tappi 42, No. 12·953-9(Dec., 1959).

4. Horio, M., and Onogi, S., J. Appl. Phys. 22, No. 7:977(1951).

5. Nolle, A. W., J. Appl. Phys. 19:753(1948).

6. Bland, D. R., and Lee, E. H., J. Appl. Phys. 26.1497(1955).

7. Horio, M., and Onogi, S., J. Appl. Phys. 22:971(1951).

8. Meredith, R., and Hsu, B.-Y., J. Polymer Sci. 61:271(1962).

9. Fujino, K., Kawai, H., and Horino, T., Textile Res. J. 25·722(1955).

10. Astatic Type M41-8 magnetic recording head from the Astatic Corporation, Conneaut, Ohio.

11. Cook's No. 2 file signal from the H. C. Cook Company, Ansonia, Conn.

12. Hewlett-Packard Model 200 J audio oscillator from the Hewlett-Packard Company, Palo Alto, California.

13. McIntosh Model MC-30, 30-watt power amplifier, Type A-116B. McIntosh Laboratory, Inc., 2 Chambers Street, Binghamton, New York.

14. Karrholm, E. M., and Schroder, B., Textile Res. J. 23:207(1953).

15. Stauff, D. W., and Montgomery, D. J., J. Appl. Phys. 26:540(1955).

16. Wink, W. A., Tappi 44:513(1961).

17. Tipton, H., J. Textile Inst. 46:T322(1955).

# PROJECT REPORT FORM

Copies to: Central Files
J. W. Swanson
G. R. Sears
S. F. Kurath
W. P. Riemen
Reading Copy

THE RHEOLOGY OF PAPERMAKING MATERIALS

A LITERATURE SURVEY*

PART I

*Literature survey was completed September 1, 1962.

# TABLE OF CONTENTS

Page

# INTRODUCTION

The material presented here is intended to serve as an introduction to the terminology and mathematical forms in current use in the study of viscoelastic materials. The subject matter is covered in two sections.

The first section on viscoelastic principles is intended to serve as a brief presentation of basic principles in the stress and strain behavior of materials. In this section we introduce the concept of the complex modulus and its application to the viscoelastic solid. A discussion of the Maxwell and Kelvin-Voigt models has also been included. The use of these models has been prompted by several factors. In spite of the fact that their use is avoided in current experimental and theoretical work, we feel that their retention is justified on the basis of their mathematical form. The relations that exist between the relaxation modulus and the complex modulus of the Maxwell model and between creep compliance and the complex compliance of the Kelvin-Voigt model are clearly demonstrated. The mathematical forms introduced by these models will become important in dealing with viscoelasticity on a phenomenological basis and in discussing the results of molecular theories on polymer viscoelasticity. Current theoretical work on wave propagation in viscoelastic media has been confined to solutions based on these elementary models. The rheological behavior of certain simple liquids can be adequately described in terms of such models. Finally, the simple Maxwell model can be profitably employed in isolating discrete relaxation times that occur in certain polymeric media.

In the second section on phenomenological viscoelasticity we take a strictly mathematical approach. While no assumption is made concerning molecular structure, this approach is extremely useful in expressing the results of

experimental observations and in correlating and interrelating experimental

results obtained through the use of various experimental techniques. Its

strength lies in the general validity of the Boltzmann superposition integral.

This section includes a survey of various approximational techniques for the

determination of relaxation and retardation distribution functions.

## VISCOELASTIC PRINCIPLES

### THE HOOKEAN SOLID

If a strain is applied to an isotropic Hookean solid, a corresponding

stress will be observed which is proportional to the applied strain, Fig. 1.

The relation between stress and strain is given by,

$$\sigma = m \epsilon \tag{1}$$

where $\sigma$ is the stress, $\epsilon$ the strain, and $\underline{m}$ the modulus. The nature of the

modulus will depend upon the manner in which the solid is strained. In

accordance with the recommendations of the Society of Rheology $(\underline{1})$, the symbol

$\underline{E}$ will be used to designate Young's modulus, $\underline{G}$ for the shear modulus, and $\underline{K}$

for the bulk modulus.

Occasionally, it is more convenient to deal in terms of compliance

relations. Accordingly, the strain is related to the corresponding stress by

the relation,

$$\epsilon = k \sigma \tag{2}$$

where $\underline{k}$ is known as the compliance.

$$m = \frac{\sigma}{\epsilon}$$
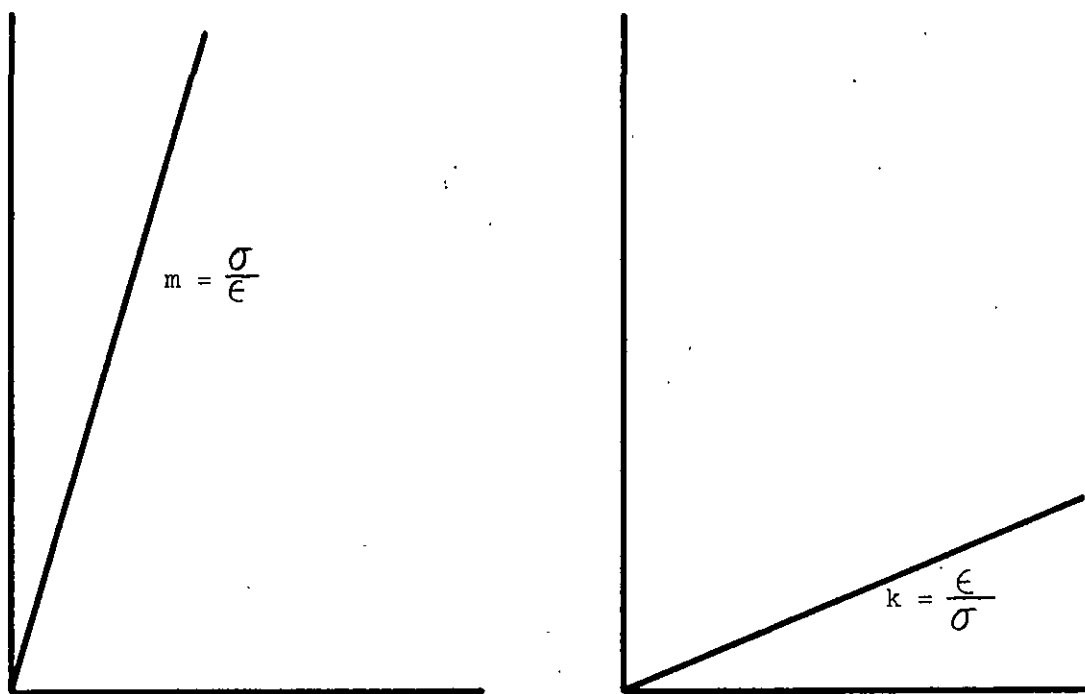
$$k = \frac{\epsilon}{\sigma}$$

Figure 1. Stress-strain Relations for a Hookean Solid

The symbol $\underline{D}$ is used for the compliance of a solid under tension, $\underline{J}$ is the shear compliance, and $\underline{B}$ is the bulk compliance. The modulus can be determined from the compliance by means of,

$$m = \frac{1}{k} \quad . \tag{3}$$

## NEWTONIAN LIQUIDS

Consider a Newtonian liquid sheared between two flat parallel plates, one fixed in space, the other moved by a tangential force, $\underline{F}$ (see Fig. 2). If $\underline{A}$ is the area of the plates, the force will give rise to a shear stress $\sigma = F/\underline{A}$ and will set up a laminar velocity distribution as indicated. The velocity, $\underline{V}$, at any point $\underline{Z}$ from the stationary plate is given by

$$V = \frac{1}{\eta} \sigma Z \tag{4}$$

where $\eta$ is the shear viscosity. Since the velocity gradient $\underline{dV}/\underline{dZ}$ equals the rate of strain $\underline{d\epsilon}/\underline{dt}$,

$$\sigma = \eta \frac{d\epsilon}{dt} \quad . \tag{5}$$

According to Equation (5), the shear stress is proportional to the rate of strain.

## THE VISCOELASTIC SOLID

Consider a sinusoidal stress, $\sigma = \sigma_o \sin \omega \underline{t}$ where $\sigma_o$ is the amplitude and $\omega$ is the circular frequency. If a sinusoidal stress is applied to a Hookean solid, a sinusoidal strain will be observed which is in phase with the applied stress, Fig. 3. This will not be true for a viscoelastic solid for it has both "liquidlike" and "solidlike" properties. If a sinusoidal stress is applied to a viscoelastic solid the resulting sinusoidal strain will be out of
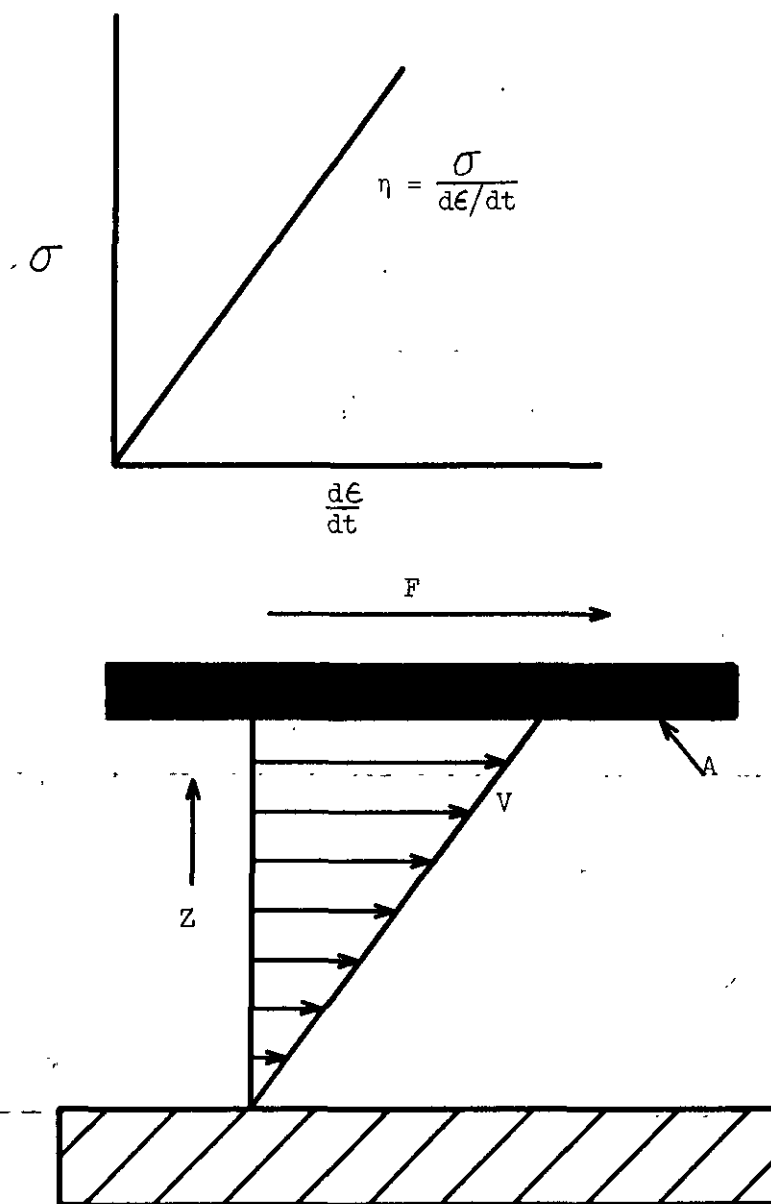
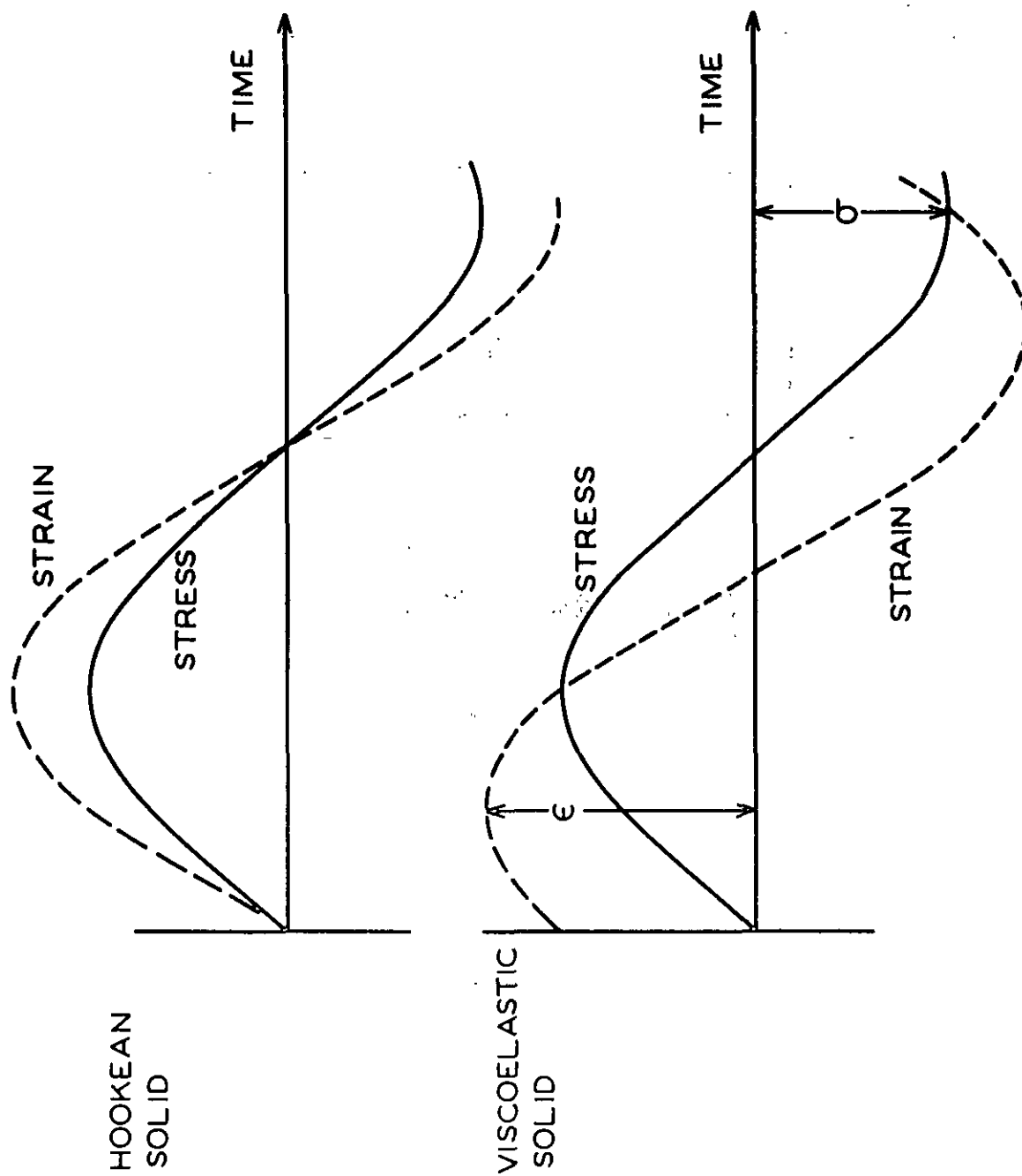Figure 2. Stress Rate-of-Strain Relations for a Newtonian Liquid

Figure 3. Stress-strain Relations for a Hookean and a Viscoelastic Material Subjected to a Sinusoidal Stress

phase with the applied stress. The relations between the sinusoidal stress and sinusoidal strain can be represented by means of a vector diagram as shown in Fig. 4. The sinusoidal stress is represented by a vector in the x-y plane. Its magnitude is given by the amplitude of the sinusoidal stress. The sinusoidal strain is represented by a vector along the x-axis. The rate of strain vector is along the y-axis. The phase difference between the stress and strain vectors is measured by the loss angle, $\Delta$.

The stress $\sigma$ can be decomposed into a solidlike and a liquidlike component. As in the case of the Hookean solid, the solidlike component is represented by a vector along the x-axis. The rate of strain vector is a vector lying along the y-axis. The phase difference between the stress and strain vectors is measured by the loss angle, $\Delta$. As in the case of the Hookean solid the solidlike component is in phase with the strain. The liquidlike stress is in phase with the rate-of-strain just as in the case of a Newtonian liquid. These basic liquidlike and solidlike features may be carried over to a consideration of the modulus. In so doing, the ratio of solidlike stress to strain is the solidlike component of the modulus, m', given by

$$\frac{\text{solidlike stress}}{\text{strain}} = m'(\omega).$$

Similarly, the liquidlike component of the modulus, m" is given by,

$$\frac{\text{liquidlike stress}}{\text{strain}} = m''(\omega).$$

As indicated in the following section, it is most convenient to write the modulus of a viscoelastic solid as a complex quantity.
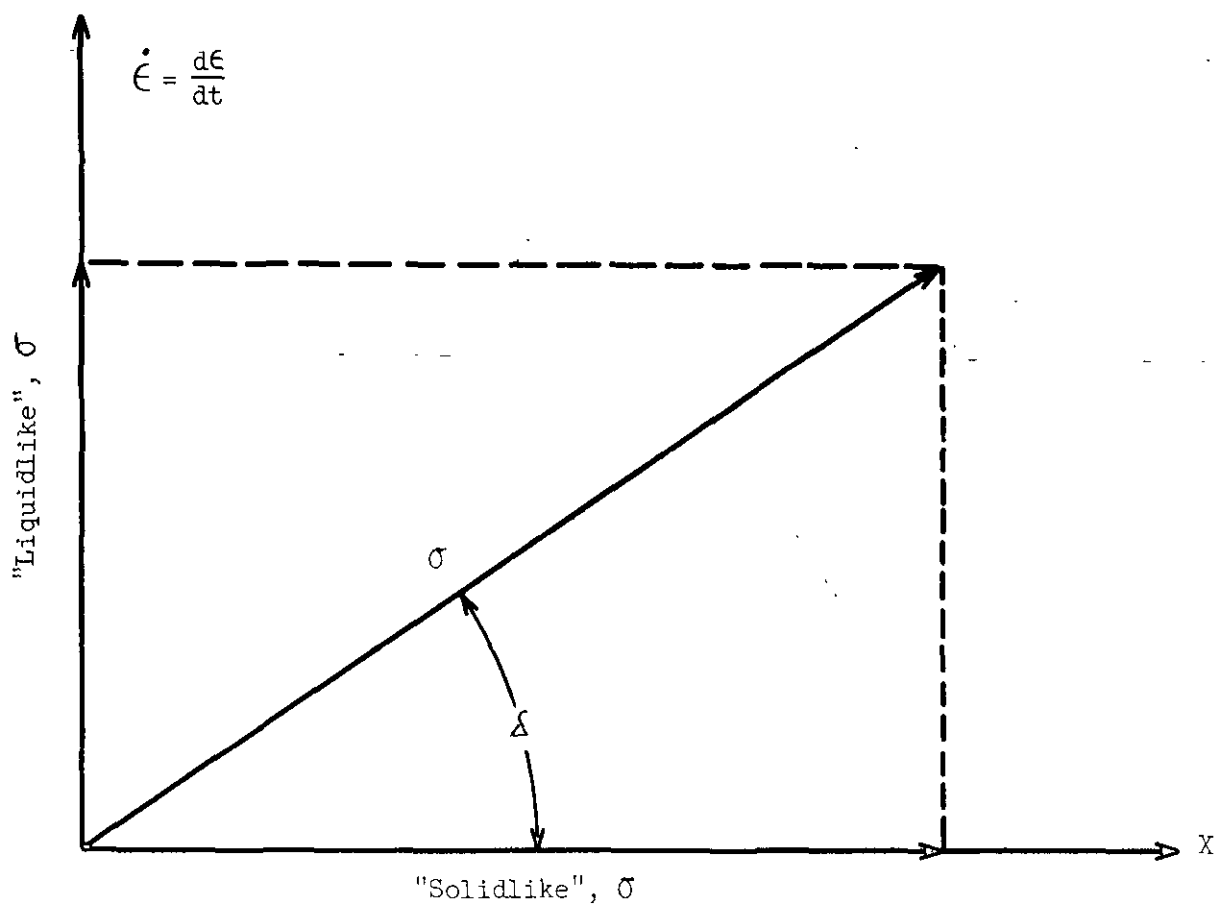
Figure 4.   Vector Representation of the Stress-strain
Relations for a Viscoelastic Solid

THE COMPLEX MODULUS AND COMPLEX COMPLIANCE

A complex number is a number of the form $U + jV$, where $U$ and $V$ are real numbers and $j$ is a number such that $j^2 = -1$. The complex number $U + jV$ can be represented by a point in a plane referred to a pair of orthogonal $X$ and $Y$-axes. The real number $U$ is agreed to represent the abscissa and the real number $V$ the ordinate of the point $(U, V)$, Fig. 5. The point $(U, V)$ may be located by the terminus of a vector $Z$ with its origin at $O$. The vector $Z$ can be thought of as the resultant of two vectors $U$ and $V$ with $U$ directed along the $X$-axis and $V$ along the $Y$-axis. One can therefore write,

$$Z = U + jV,$$

where $U$ is the real part of the complex number $Z$ and $jV$ is the imaginary part. If $(r, \theta)$ are the polar co-ordinates of the point $(U, V)$, then

$$U = r \cos \theta \quad , \quad V = r \sin \theta$$

and

$$r = (U^2 + V^2)^{1/2} \text{ and } \theta = \tan^{-1} \frac{V}{U} .$$

The number $r$ is called the modulus or absolute value, and $\theta$ is called the argument or amplitude of the complex number $Z = U + jV$. The modulus, $r$, is often written using absolute value signs, that is

$$r = |Z| = |U + jV| = (U^2 + V^2)^{1/2}$$

and the argument $\theta$ as, $\theta = \arg Z$.

The strain on a viscoelastic body can be written as,

$$\epsilon = \epsilon_o \, e^{j\omega t} \tag{6}$$

$$\epsilon = \epsilon_o \, [\cos \omega t + j \sin \omega t]. \tag{7}$$

The strain can be represented in the complex plane as a vector of magnitude $\epsilon_o$ which makes an angle $\omega t$ with the x-axis, Fig. 6. The x and y components of the vector are $\epsilon_o \cos \omega t$ and $\epsilon_o \sin \omega t$, respectively. The rate-of-strain may be obtained by differentiation of (6) to yield,

$$\dot{\epsilon} = \frac{d\epsilon}{dt} = j\omega \epsilon_o e^{j\omega t} \tag{8}$$

or,

$$\dot{\epsilon} = \epsilon_o \, (j\omega \cos \omega t - \omega \sin \omega t). \tag{9}$$

It is thus seen that $\dot{\epsilon}$ can be represented as a vector in quadrature with the strain. The stress likewise can be written as,

$$\sigma = \sigma_o \, e^{j(\omega t + \Delta)} \tag{10}$$

or, $$\sigma = \sigma_o \, [\cos(\omega t + \Delta) + j \sin(\omega t + \Delta)]. \tag{11}$$

The stress can also be represented as a vector in Fig. 6. It should be noted that the entire diagram rotates counterclockwise about the orgin with an angular velocity $\omega$. If it is now agreed to keep $\epsilon$ along the real or x-axis, then the stress, strain and rate-of-strain vectors are given by Fig. 4.

The modulus of a viscoelastic solid can be written as a complex quantity, called the complex modulus. The complex modulus, m*, is given by,

$$m^*(\omega) = m'(\omega) + jm''(\omega) = \frac{\text{sinusoidal stress}}{\text{sinusoidal strain}} \tag{12}$$

where $\underline{m}'$ is the real or solidlike component of the complex modulus and $m''$ is the imaginary or liquidlike component. The liquid nature of $m''$ is revealed by writing,

$$m''(\omega) = \omega\eta'(\omega) \tag{13}$$

where $\eta'(\omega)$ is known as the dynamic viscosity.

Another important relation is the mechanical loss tangent, $\tan \Delta$, given by,

$$\tan \Delta = \frac{m''(\omega)}{m'(\omega)} = \frac{\omega\eta'(\omega)}{m'(\omega)} = \frac{\text{energy lost/cycle}}{\text{energy stored/cycle}} \quad . \tag{14}$$

This relation is of considerable importance since it gives the ratio of energy lost to energy stored and as such is a measure of the resilience of the material.

Just as it is possible to speak of the viscosity of a liquid it is possible to define a complex viscosity for a viscoelastic solid. The complex viscosity, $\eta^*(\omega)$, is given by,

$$\eta^*(\omega) = \eta'(\omega) - j\eta''(\omega) = \frac{\text{stress}}{\text{rate-of-strain}} \tag{15}$$

where $\eta'(\omega)$ is the real or liquidlike component of the complex viscosity and $\eta''(\omega)$ is the imaginary or solidlike component.

The following relations exist between the complex modulus and the viscosity. Equation (8) can be written as,

$$\text{rate-of-strain} = j\omega \text{ (strain)}$$

and
$$\frac{m^*(\omega)}{\eta^*(\omega)} = \frac{\text{rate-of-strain}}{\text{strain}} = j\omega, \tag{16}$$

or $\qquad m^*(\omega) = j\omega\eta^*(\omega)$ . $\hspace{4cm}$ (17)

A complex compliance can also be obtained for a viscoelastic solid. The

complex compliance $\underline{k}^*(\omega)$ is related to the complex modulus by,

$$k^*(\omega) = \frac{1}{m^*}(\omega) \hspace{4cm} (18)$$

By substituting (12) into (18) one has,

$$k^*(\omega) = k'(\omega) - jk''(\omega) \hspace{4cm} (19)$$

where the real component of the complex compliance, $\underline{k}'$, and the imaginary

component, $\underline{k}''$, are given by,

$$k'(\omega) = \frac{(m')}{(m')^2 + (m'')^2}$$

and $\qquad k''(\omega) = \frac{(m'')}{(m')^2 + (m'')^2}$ . $\hspace{3cm}$ (20)

The vector diagrams corresponding to the complex modulus and the complex

compliance are given in Fig. 7.

All of the complex relations given in this section are used

extensively in the physics of viscoelastic materials. They are experimentally

observable quantities and are exceptionally useful in interpreting mechanical

properties in terms of molecular motion. It is through the complex quantities

that modern molecular theories of viscoelasticity are most readily tested.

THE MAXWELL SOLID

In the older literature on viscoelasticity considerable effort was

devoted to devising mechanical models to represent the mechanical behavior

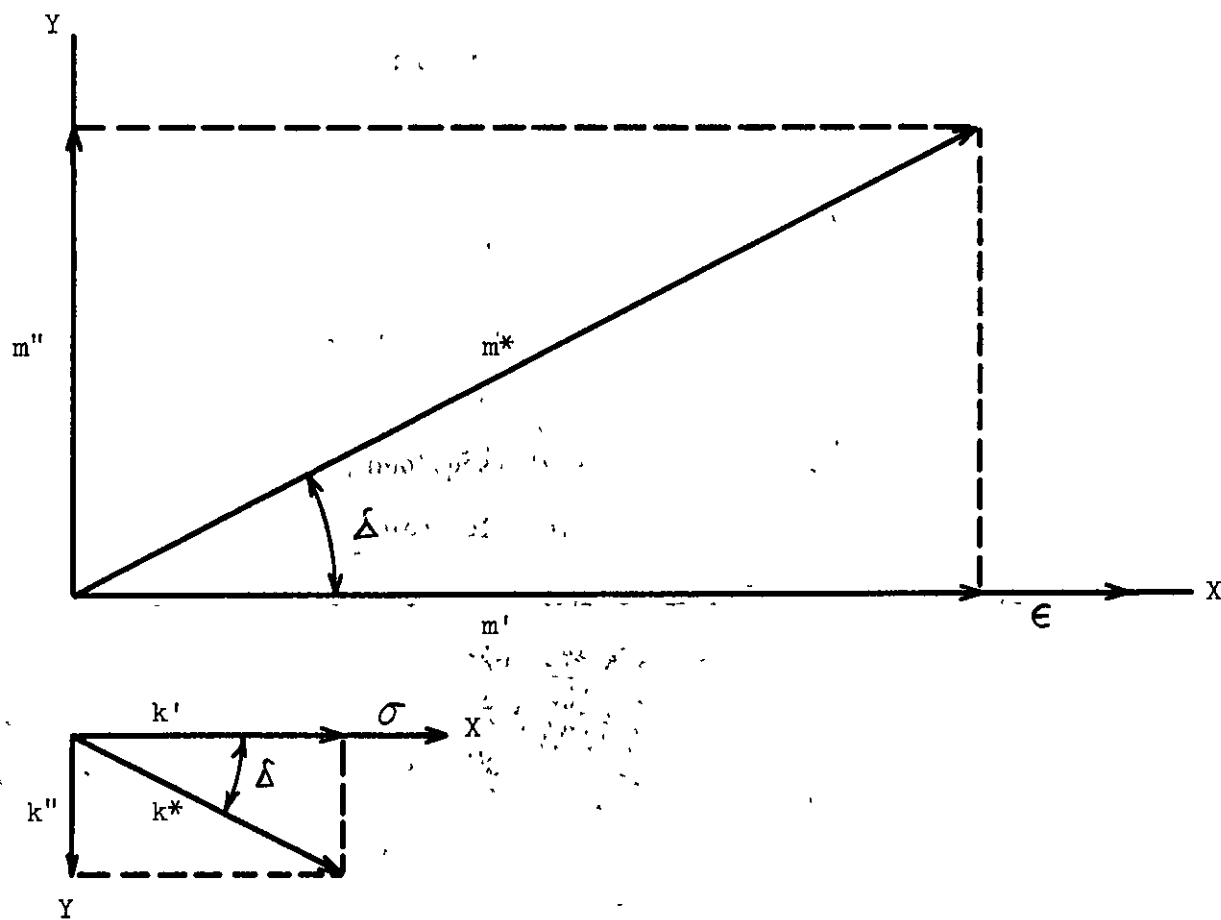of a viscoelastic body. While the use of mechanical models consisting of

Figure 7. Vector Diagrams for the Complex Modulus and the Complex Compliance

springs and dashpots cannot be justified on the basis of what we now know about

the molecular origin of viscoelasticity, their inclusion in the present section

is justified on the basis of their mathematical form which is now observed in the

modern molecular theories. Apart from historical interest, the reader will find

the mathematical form of these models useful in understanding the mathematically

more complex phenomenological theories of viscoelasticity.

In 1867 Maxwell (2) suggested that the stress and strain of a real

solid could be related by the equation,

$$\frac{d\epsilon}{dt} = \frac{1}{m}\frac{d\sigma}{dt} + \frac{\sigma}{\eta} \quad , \tag{21}$$

while a purely elastic solid obeys Equation (1). One of the common experiments

that can be carried out on viscoelastic systems is the stress relaxation

experiment. An initially unstrained material is suddenly strained and held at

constant strain while the time decay of stress is observed. If this experiment

is performed on a Maxwell solid, $\epsilon = 0$ at $t = 0$ while for $t > 0$, $\epsilon$ is constant

and $d\epsilon/dt = 0$. For $t > 0$, Equation (21) becomes,

$$\frac{1}{m}\frac{d\sigma}{dt} + \frac{\sigma}{\eta} = 0. \tag{22}$$

Upon integration this becomes,

$$\sigma(t) = \sigma_o e^{-mt/\eta} \quad , \tag{23}$$

or after dividing by the strain $\epsilon$ and employing Equation (1),

$$m(t) = m e^{-t/\tau} \tag{24}$$

where $\tau = \eta/m$ is the relaxation time. At times short compared to $\tau$, the

material behaves as an elastic solid. For long times the behavior is that of

a viscous liquid and the modulus decays to zero. The Maxwell solid is often

represented by means of a mechanical model consisting of a spring in series

with a viscous element of dashpot, Fig. 8. The spring is assumed to be a

Hookean spring while the dashpot can be considered to be a piston which is

drawn through a Newtonian liquid.

The relaxation of stress in an actual solid does not, in general,

follow that of the Maxwell solid and schemes have been devised to represent

the actual solid by means of a series of Maxwell elements in parallel with a

Hookean spring, Fig. 9. The mathematical expression for stress relaxation is

therefore given by the series summation,

$$m(t) = \sum^{i} m_i \, e^{-t/\tau_i} + m_e \qquad (25)$$

where $m_e$ is the equilibrium modulus of the parallel spring. The summation

extends over the (i) Maxwell elements in parallel and $(m_i)$ refers to the modulus

at zero time for element (i). The use of a series of parallel elements is,

of course, an arbitrary procedure. It is introduced here since molecular

theories of viscoelasticity predict precisely this form and in addition provide

for the distribution of relaxation times, $\tau_i$.

## THE DYNAMIC MAXWELL ELEMENT

If a sinusoidal stress is applied to a Maxwell solid, it is possible

to obtain an expression for the complex modulus, $m^*$, where the real and

imaginary components are, respectively,

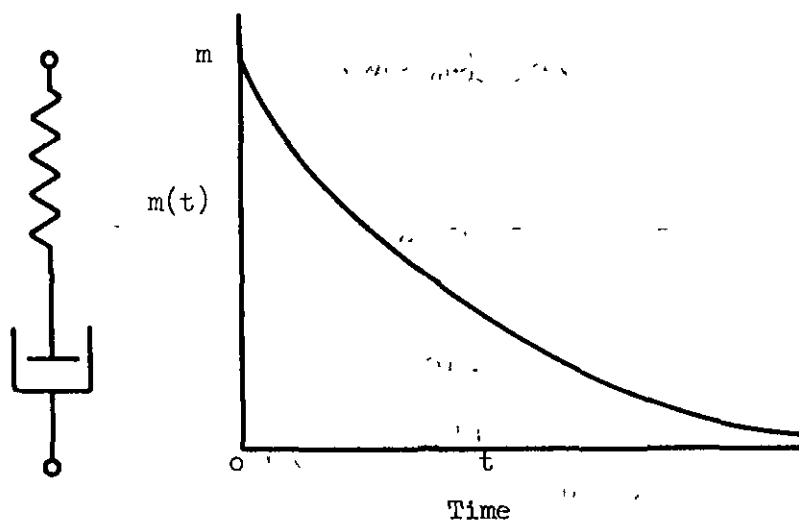$$m'(\omega) = m\frac{\omega^2 \tau^2}{1 + \omega^2 \tau^2} \qquad (26)$$

Figure 8. Mechanical Model for the Maxwell Solid and Its Behavior
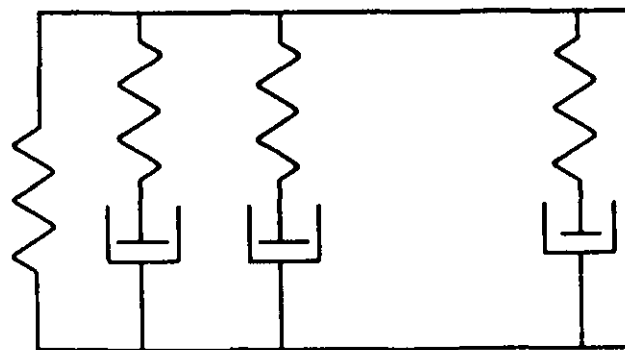in Stress Relaxation



Figure 9. The generalized Maxwell element

and
$$m''(\omega) = m \frac{\omega \tau}{1 + \omega^2 \tau^2} \tag{27}$$

where $\omega$ is the circular frequency and $\tau$ is the relaxation time. The frequency

response of the dynamic Maxwell element is shown in Fig. 10, where $\underline{m}'$ and $\underline{m}''$

are given as a function of $\omega \tau$. At low frequency where $\omega \tau \langle 1$, both $\underline{m}'$ and $\underline{m}''$

are small. As the frequency is increased to the point where $\omega \tau = 1$, both

components have a value of $\underline{m}/2$, however, $\underline{m}''$ is at a maximum and $\underline{m}'$ is at an

inflection point. At high frequencies $\underline{m}''$ will become zero and $\underline{m}'$ will approach

the value $\underline{m}$. The behavior of the Maxwell solid in stress relaxation is also

given for comparison. It should be noted that once the relaxation time is

known the time dependent behavior is established for both dynamic and stress

relaxation experiments.

As in the case of stress relaxation the response of an actual

viscoelastic solid may be represented by a series of Maxwell elements in

parallel with a Hookean spring resulting in,

$$m'(\omega) = \sum_i m_i \frac{\omega^2 \tau_i^2}{1 + \omega^2 \tau_i^2} + m_e \tag{28}$$

and
$$m''(\omega) = \sum_i m_i \frac{\omega \tau_i}{1 + \omega^2 \tau_i^2} \tag{29}$$

for the real and imaginary components of the complex modulus. As in the case

of stress relaxation molecular theories predict this mathematical form for the

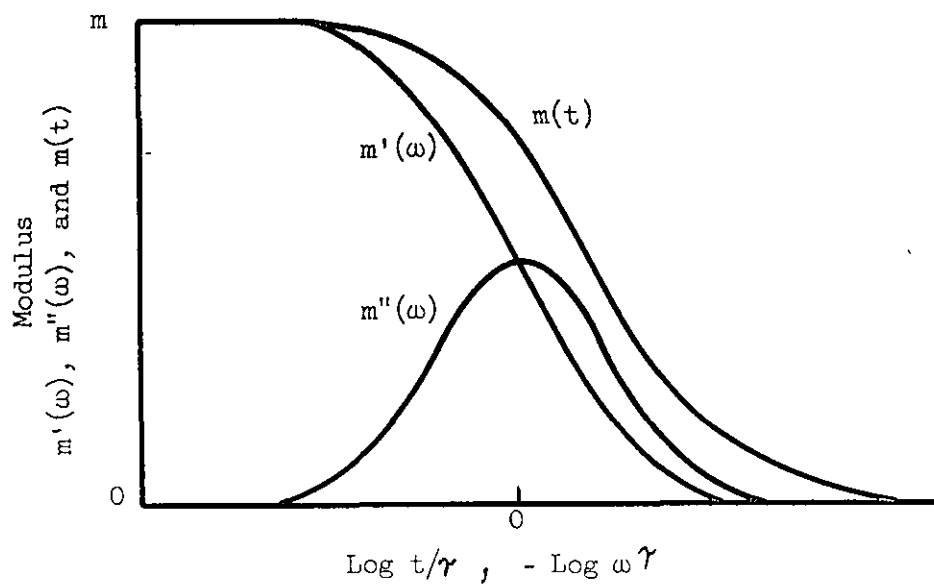complex modulus and predict the distribution of relaxation times.

Figure 10. Response of the Maxwell Solid

THE KELVIN-VOIGT MODEL

A rather simple mathematical model can be constructed for the creep of a viscoelastic solid. This representation was first proposed in 1875 by Kelvin (3) and independently in 1890 by Voigt (4). The stress on a Kelvin-Voigt solid is given by,

$$\sigma = \eta \frac{d\epsilon}{dt} + m\epsilon, \tag{30}$$

and the mechanical model is represented in Fig. 11 as a Hookean spring in parallel with a Newtonian dashpot. An important feature of this model is that it is impossible to cause an instantaneous deformation. If the stress is constant, Equation (30) can be integrated to yield,

$$\epsilon = \frac{\sigma}{m} (1 - e^{-t/\tau}) \tag{31}$$

where $\tau$ is the retardation time given by $\tau = \frac{\eta}{m}$. Relation (31) can be written in terms of compliances as

$$k(t) = k(1 - e^{-t/\tau}), \text{ with } k = \frac{1}{m}. \tag{32}$$

The response of the Kelvin-Voigt solid is shown in Fig. 11. The compliance increases with time and eventually approaches the value $k$ at long times. Most materials exhibit a finite initial strain and some have a steady flow viscosity in addition so that the Kelvin-Voigt solid is inadequate for most materials.

In order to describe an actual solid in terms of mechanical models it is necessary to use a sequence of Kelvin-Voigt elements in series with a single Maxwell element, Fig. 12. The corresponding mathematical expression is

$$k(t) = k_g + \frac{t}{\eta} + \sum^{i} k_i (1 - e^{-t/\tau_i}), \tag{33}$$
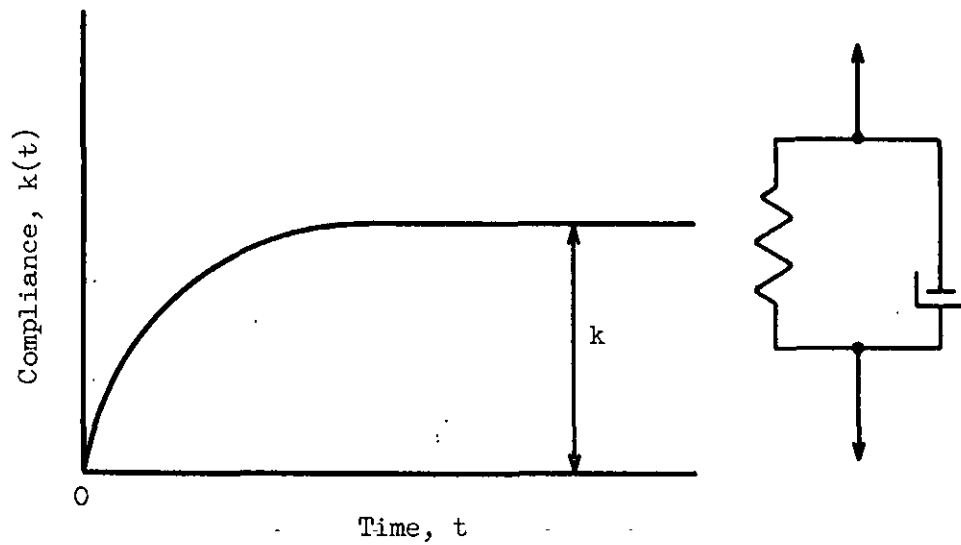
Figure 11.   Creep Compliance for the Kelvin-Voigt Solid
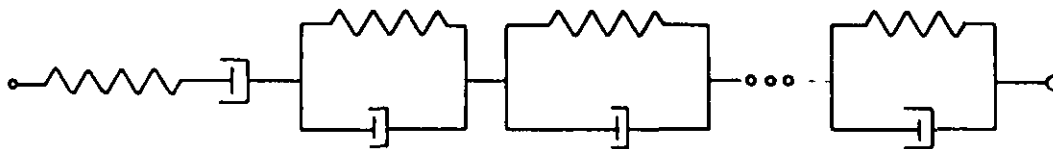


Figure 12.   The Generalized Kelvin-Voigt Model of a Viscoelastic
             Solid

where $k_g$ is the instantaneous compliance and $\eta$ the steady flow viscosity. The form of this equation is, of course, arbitrary but we have introduced it in the present form since it anticipates results obtained from the phenomenological and mathematical basis of viscoelasticity.

## THE DYNAMIC KELVIN-VOIGT MODEL

If a sinusoidal stress is applied to a Kelvin-Voigt model, one can speak in terms of the complex compliance $k^*(\omega)$, in which case $k'(\omega)$ the real, and $k''(\omega)$ the imaginary components are given by

$$k'(\omega) = k \frac{1}{1 + \omega^2 \tau^2} \tag{34}$$

and

$$k''(\omega) = k \frac{\omega \tau}{1 + \omega^2 \tau^2} . \tag{35}$$

The creep compliance, and the real and imaginary components of the complex compliance are given in Fig. 13. The creep compliance increases from a value of zero at short times to the value, $k$, the compliance of the spring at long times. The real component of the complex compliance increases to a value of $\frac{1}{2}k$ at $\omega \tau = 1$ and then to a maximum value of $k$ at high frequency. The imaginary component is zero at low frequency, reaches a maximum of $\frac{1}{2}k$ at $\omega \tau = 1$ and again decreases to zero at high frequencies.

The response of the generalized Kelvin-Voigt model can be expressed as a complex compliance with:
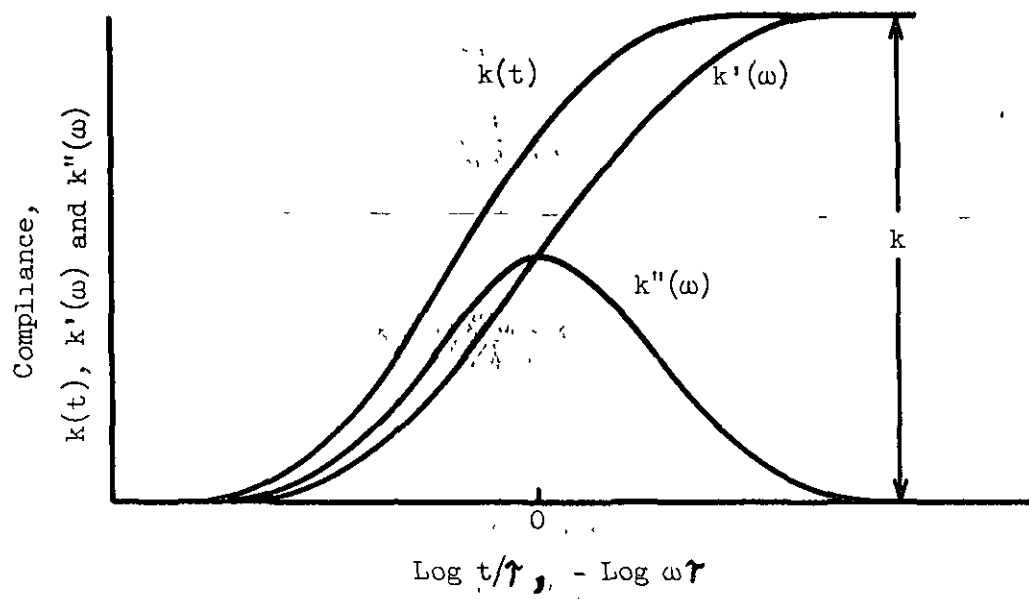
Figure 13    Response of the Kelvin-Voigt Solid

$$k'(\omega) = \sum_i k_i \frac{1}{1 + \omega^2 \tau_i^2} + k_g \tag{36}$$

and

$$k''(\omega) = \sum_i k_i \frac{\omega \tau_i}{1 + \omega^2 \tau_i^2} + \frac{1}{\omega\eta} . \tag{37}$$

This mathematical structure will appear again in the phenomenological and mathematical basis of viscoelasticity.

## THE PHENOMENOLOGICAL APPROACH TO VISCOELASTICITY

### THE BOLTZMANN SUPERPOSITION PRINCIPLE

The phenomenological approach to viscoelasticity has played an important role in the analysis of time dependent stress and strain measurements. The underlying principle was first formulated as early as 1874 by Boltzmann [5] as his principle of superposition. He suggested that the mechanical behavior of a solid is a function of its entire previous loading history. When a specimen has undergone a series of deformations, the effect of each deformation is assumed to be independent of the others. Accordingly, the resultant behavior can be calculated by a simple addition of effects that would occur if the deformations had taken place independently. This assumption is the substance of the Principle of Superposition.

This simple assumption makes it possible to compare the results of measurements obtained by different experimental techniques. In addition, it shows under what conditions an arbitrary strain history may be related to the corresponding stress history. For example, this principle can be used to predict the results of a creep experiment from a stress relaxation experiment.

THE SUPERPOSITION INTEGRAL

There are several ways to carry out a formulation of the super-position principle. We have chosen to carry out the formulation in terms of the linear superposition integral. Once the Boltzmann principle is stated in this manner the rigor of a well formulated mathematical structure can be applied. This mathematical basis of viscoelasticity is discussed in detail by Gross (6) and reviewed by Ferry (7).

Leaderman (8) gives three derivations of the Boltzmann Superposition Principle. This includes a derivation due to Becker (9) and Boltzmann's presentation (5). The derivation given here is based on Leaderman's "first method" but is in a slightly more general form.

The response of a specimen of material subjected to a stress relaxation experiment is given by,

$$\sigma = [m_e + m(t - u)]\epsilon \qquad \begin{array}{ll} \epsilon = 0 & t < u \\ \epsilon = \epsilon_0 & t > u \end{array} \qquad (38)$$

where $m(t - u)$ is the relaxation modulus function or memory function and $m_e$ is the equilibrium elastic modulus. The strain $\epsilon$ is zero for time $t < u$ and equal to a constant value $\epsilon_0$ for $t > u$. By agreement, the relaxation modulus function is zero for $t < u$ and equal to $m(t - u)$ for $t > u$. The response of the specimen of material is given in Fig. 14 as the ratio of stress to strain. At time $u$ the specimen is suddenly strained and the relaxation modulus function $m(t - u)$ decays to zero at infinitely long times.

The creep response of a specimen of material under a constant applied stress is given by,

$$\epsilon = [k_g + \frac{t - u}{\eta} + k(t - u)] \sigma \qquad \begin{array}{ll} \sigma = 0 & t < 0 \\ \sigma = \sigma_o & t \geq 0 \end{array} \qquad (39)$$

where $k_g$ is the instantaneous compliance, $\eta$ the viscosity coefficient and $k(t - u)$ is the creep compliance function. The specimen is initially unstressed. Later at some arbitrary time $u$ the material is subjected to a constant stress $\sigma_o$. It is understood that the creep compliance function is zero at time $u$ and increases to a finite limiting value at infinite time. The response of the specimen in creep is shown in Fig. 15.

The response of a linear viscoelastic material to an arbitrary strain pattern may be described as follows, Fig. 16. The time is divided into increments $\Delta u$ and the strain is approximated by a series of incremental steps,

$$\left[\frac{\Delta \epsilon(u)}{\Delta u}\right]\Delta u .$$

The stress response to an incremental step started at time $u$ is given by,

$$\left[\frac{\Delta \epsilon(u)}{\Delta u}\right] \Delta u [m(t - u) + m_e] .$$

The total stress response at any time $t$ is then given by,

$$\sigma(t) = \sum_{t = \Delta u}^{t} \frac{\Delta \epsilon(u)}{\Delta u} [m(t - u) + m_e]\Delta u, \qquad (40)$$

with the strain $\epsilon(-\infty)$ taken as zero. If $\Delta u$ is allowed to approach zero, the sum has the limit,

$$\sigma(t) = \int_{-\infty}^{t} \frac{d\epsilon(u)}{du} [m(t - u) + m_e]du . \qquad (41)$$
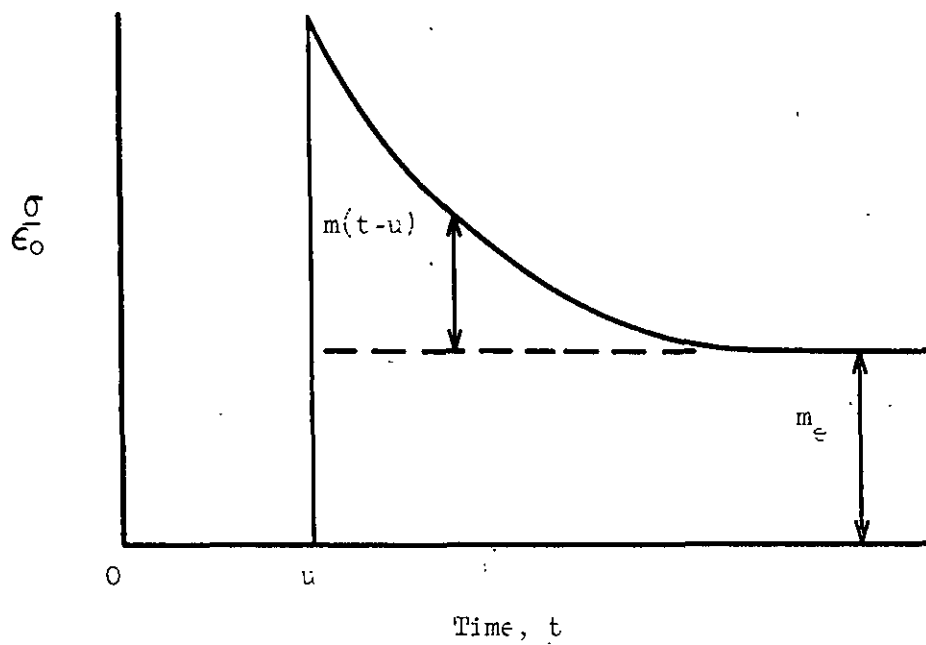
Figure 14. Stress Relaxation of a Viscoelastic Solid
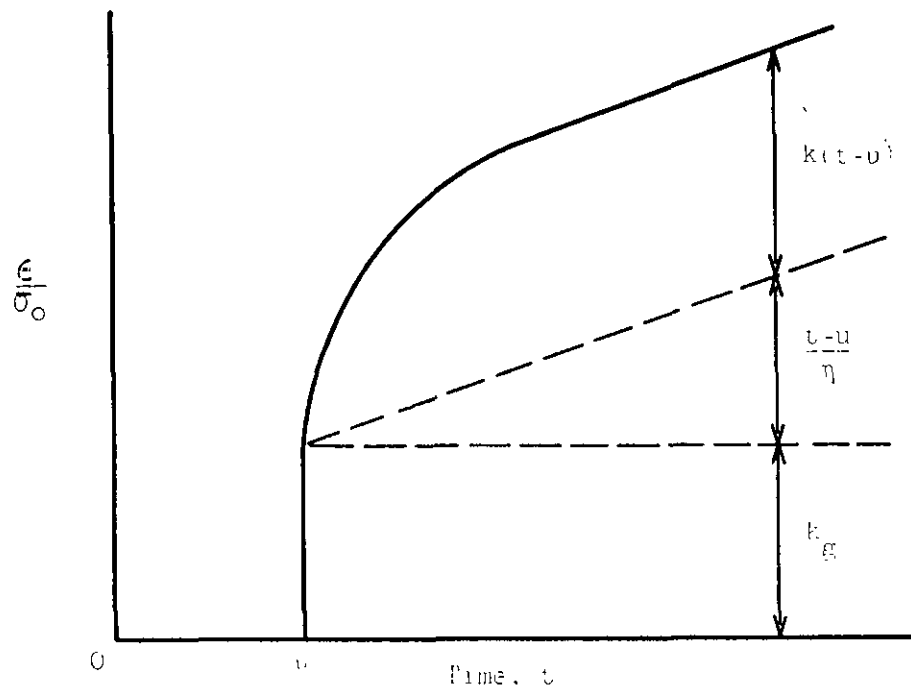


Figure 15. Creep of a Viscoelastic Solid
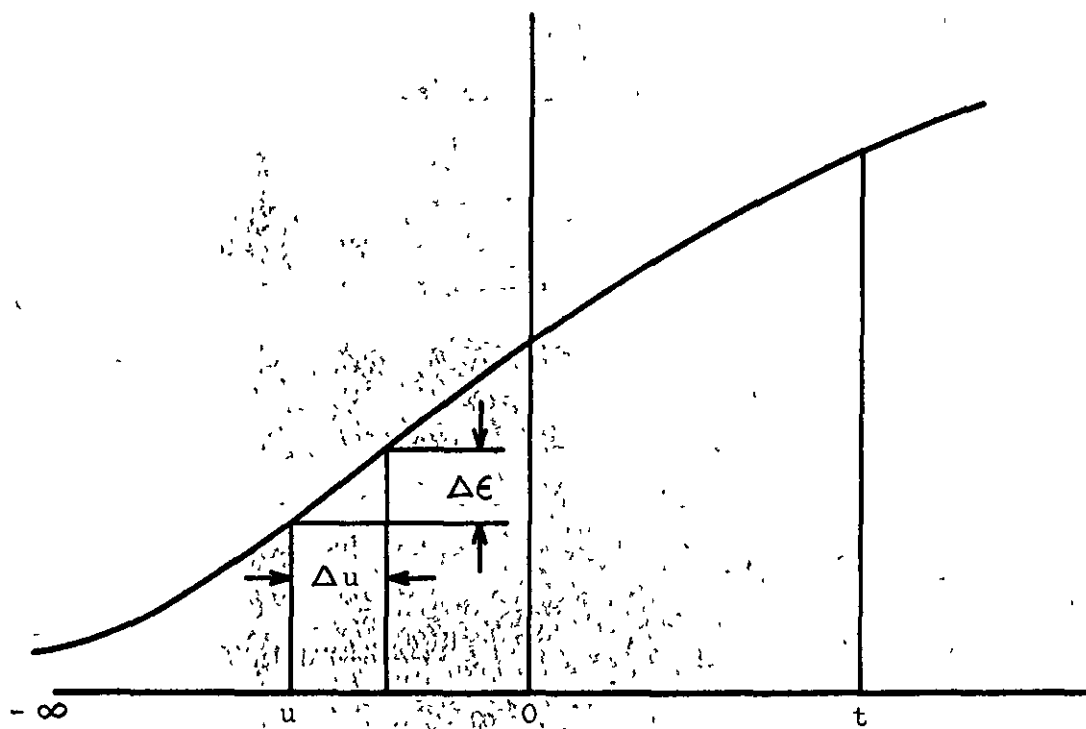
Figure 16. Arbitrary Strain History on a Viscoelastic Solid

By using considerations similar to those used in deriving (41), the total creep

response due to an arbitrary stress history is given by,

$$\epsilon(t) = \int_{-\infty}^{t} \frac{d\sigma(u)}{du} [k_g + \frac{t - u}{\eta} + k(t - u)]du. \qquad (42)$$

The integrals (41) and (42) taken together, are known as the principle of

superposition. The equations are, of course, not independent of one another.

Mathematically they are known as Duhamel's integrals (6). The principle of

superposition is important in many areas of physics and finds application in

the study of electrical networks and dielectrics.

## MATHEMATICAL RELATIONS

The results of mechanical measurements on the modulus of a viscoelastic

material can be expressed as,

$$m(t) = m_e + \int_{-\infty}^{\infty} H(\tau)e^{-t/\tau} \, d \ln \tau \qquad (43)$$

for stress relaxation or as,

$$m'(\omega) = m_e + \int_{-\infty}^{\infty} \frac{H(\tau)\omega^2\tau^2}{1 + \omega^2\tau^2} \, d \ln \tau \qquad (44)$$

and

$$m''(\omega) = \int_{-\infty}^{\infty} \frac{H(\tau)\omega\tau}{1 + \omega^2\tau^2} \, d \ln \tau \qquad (45)$$

for a dynamic experiment. Equations (43), (44), and (45) are linear integral

equations of the convolution type. It should be noted that time appears on

both sides of (43) and $\omega$ on both sides of (44) and (45). The modulus on the

left is the experimentally accessible quantity and is a function of time or

frequency. The function $\underline{H}(\Upsilon)$ is the relaxation distribution function and is an unknown function which is to be determined from the modulus. By comparing (43) with (25), and (44) and (45) with (28) and (29), it is seen that $\underline{H}(\Upsilon)$ is just the contribution to the modulus from Maxwell elements lying between $\underline{\ln} \Upsilon$ and $\underline{\ln} \Upsilon + \underline{d} \ \underline{\ln} \Upsilon$. These equations are simply the integral expressions for the generalized Maxwell model.

If the Boltzman superposition principle applies, then (43), (44), and (45) are related through $\underline{H}(\Upsilon)$ since this function will be identical when determined from each relation. Experimental techniques which determine both $\underline{m}'(\omega)$ and $\underline{m}''(\omega)$ are quite powerful since $\underline{H}(\Upsilon)$ can be determined from both components and this yeilds internal verification of the superposition principle. It is apparent that this principle also makes it possible to compute the results of a stress relaxation experiment from the results of a dynamic experiment.

Close relations also exist between creep experiments and dynamic experiments. The creep compliance of a linear viscoelastic material is given by,

$$k(t) = k_g + \int_{-\infty}^{\infty} L(\Upsilon)[1 - e^{-t/\Upsilon}] d \ln \Upsilon + \frac{t}{\eta} \tag{46}$$

and the components of the complex compliance by,

$$k'(\omega) = k_g + \int_{-\infty}^{\infty} \frac{L(\Upsilon)}{1 + \omega^2 \Upsilon^2} d \ln \Upsilon \tag{47}$$

and

$$k''(\omega) = \frac{1}{\omega \eta} + \int_{-\infty}^{\infty} \frac{\omega \Upsilon L(\Upsilon)}{1 + \omega^2 \Upsilon^2} d \ln \Upsilon \tag{48}$$

Here the similarity of these equations to the Kelvin-Voigt model of a viscoelastic solid should be noted. As in the case of the modulus, time

appears on both sides of Equation (46) and ω on both sides of (47) and (48). The experimental quantities are on the left side of the equations and the unknown retardation spectrum $L(\Upsilon)$ is to be determined. The creep compliance, Equation (46), represents a continuous series of Kelvin-Voigt elements and (47) and (48) a continuous series of dynamic Kelvin-Voigt elements. The retardation distribution function, $L(\Upsilon)$, simply represents the contribution to the compliance from elements with retardation times lying between $\ln \Upsilon$ and $\ln \Upsilon + d \ln \Upsilon$. Here again if the superposition principle applies the results of a dynamic experiment can be used to calculate the behavior of a material under creep.

In view of the fact that compliances and moduli are related, by Equations (18) and (20), it is not surprising to find that relaxation spectra and retardation spectra are also related. Direct relations between the spectra are discussed by Gross (6) and by Ferry (7), and the reader is referred to these sources. A discussion will not be included here since retardation and relaxation spectra are not interconverted in general practice.

The practice of describing experimental results in terms of continuous spectra has certain advantages over the use of the generalized Maxwell and Kelvin-Voigt models. The results of any stress relaxation experiment may be described in terms of the generalized Maxwell element, provided only that the results decrease monotonically with time. The experimental results can be fitted to any degree of accuracy by including a sufficient number of elements in the model. A given choice of elements is, however, not unique and hence, it is not possible to associate relaxation times with molecular motion. The generalized Maxwell and Kelvin-Voigt elements are therefore not useful for theoretical interpretation. The advantage of the

continuous relaxation and retardation spectra lies in the fact that the spectra are unique and therefore amenable to theoretical interpretation.

METHODS FOR OBTAINING RELAXATION SPECTRA

The utility of the equations in the preceding section depends on the ability to determine the distribution functions $\underline{H}(\gamma)$ and $\underline{L}(\gamma)$. As the result of experimental observation, it is possible to determine the moduli or compliances of a viscoelastic material as a function of time or frequency. The problem is then to determine the value of the distribution function under the integral sign. In general, the modulus will not be a simple function of time or frequency and one is required to devise approximational techniques in order to determine relaxation distribution functions from an arbitrary modulus time or frequency curve. There are a number of methods for determining relaxation distribution functions and these are discussed by Ferry $(\underline{7})$. We have selected several for discussion here because of their usefulness to specific materials used in papermaking. The first order approximations discussed by Andrews $(\underline{10})$ are given here because of their applicability to pulp and paper. The higher approximation method of Ferry and Williams $(\underline{11})$ is discussed because of the ease with which spectra can be determined from experimental data. The complicated and more accurate method of Roessler $(\underline{12})$ is included since it is not discussed in detail by Ferry $(\underline{7})$. Finally, the recent method of Tobolsky and Murakami $(\underline{13})$ is included since it enables one to isolate discreet relaxation times under certain conditions.

## Simple Approximational Methods

A simple approximation of the relaxation distribution function can be obtained in the following way $(\underline{10})$. Equation (43) is differentiated under the integral sign with respect to time to yield,

$$- \frac{dm(t)}{d \log} = \int_{-\infty}^{\infty} H(\tau) \left[ \frac{2.303te^{-t/\tau}}{\tau} \right] d \log \tau \qquad (49)$$

where the term in square brackets can be considered as an intensity function which specifies the contribution of various regions of $\underline{H}(\tau)$ to the value of the integral. When the intensity function is plotted versus $(\log \tau - \log t)$ it is seen to have a fairly sharp maximum at $\tau = t$ and falls rapidly to zero on either side. If $\underline{H}(\tau)$ is constant in the neighborhood of time, $\underline{t}$, it may be removed from under the integral sign and since

$$\int_{-\infty}^{\infty} \left[ \frac{2.303 \, te^{-t/\tau}}{\tau} \right] d \log \tau = 1, \qquad (50)$$

we get

$$- \frac{dm(t)}{d \log t} = H(\tau) \Big|_{\tau = t} \qquad (51)$$

thus providing a first approximation to the distribution function.

A similar situation exists with respect to the components of the complex modulus. Equation (44) can be differentiated under the integral sign with respect to $1/\omega$ with the result,

$$- \frac{d \, m'(\omega)}{d \log 1/\omega} = \int_{-\infty}^{\infty} H(\tau) \left[ \frac{4.606 \, \omega^2 \tau^2}{(1+\omega^2\tau^2)^2} \right] d \log \tau . \qquad (52)$$

As in the case of stress relaxation the intensity function in square brackets has a fairly sharp peak at $1/\omega = \tau$ and decreases to zero on either side. Again, if $\underline{H}(\tau)$ is nearly constant in the neighborhood of $\tau = 1/\omega$ it can be brought out from under the integral sign. The remaining integral is,

$$- \int_{-\infty}^{\infty} \left[ \frac{4.606 \, \omega^2 \tau^2}{(1+\omega^2\tau^2)^2} \right] d \log \tau = 1 \qquad (53)$$

and one has,

$$- \frac{dm'(\omega)}{d \log 1/\omega} = H(\gamma)\Big|_{\gamma = \frac{1}{\omega}} . \tag{54}$$

The imaginary component of the modulus (45) already has a peaked function under the integral. The function

$$\left[\frac{\omega \gamma}{1 + \omega^2 \gamma^2}\right] \tag{55}$$

has a peak at $\gamma = 1/\omega$ and is a symmetrical curve. If $\underline{H}(\gamma)$ is assumed constant in the neighborhood of $\gamma = 1/\omega$ it may be brought out from under the integral sign. The remaining integral is

$$\int_{-\infty}^{\infty} \left[\frac{\omega \gamma}{1 + \omega^2 \gamma^2}\right] d \log \gamma = \frac{\pi}{4.606} , \tag{56}$$

and one gets the approximation,

$$m''(\omega) = \frac{\pi}{4.606} H(\gamma)\Big|_{\gamma = 1/\omega} . \tag{57}$$

Second order approximations ($\underline{10}$) can be obtained by assuming a relaxation distribution function of the form,

$$H(\gamma) = \alpha + \beta (\log \gamma - \log t) \tag{58}$$

where $\alpha$ is the value of $\underline{H}(\gamma)$ at $\gamma = \underline{t}$. This leads to the results,

$$H(\gamma)\Big|_{t = \gamma} = - \frac{d\, m(t)}{d\, \log t} + 0.251 \frac{d^2 m(t)}{d \log t^2} , \tag{59}$$

for stress relaxation. When (58) is substituted into (52) the contribution of the second term of (58) to the slope of (54) is zero. This results from the symmetry of the itensity function about its peak at $\gamma = \underline{t}$. This means that (54) is second approximation as well as first. A similar situation exists

with respect to (57) and hence, this also is a second order approximation as well as first. Other second and higher order approximations are given by Schwarzl and Staverman (14), Okano (15), and Fujita (16), and an iterative numerical method is outlined by Roesler and Twyman (17). A method that does not involve the measurement of slopes is described by Ninomiya and Ferry (18).

## Ferry-Williams Method

The method of Ferry and Williams (19) yields the following relation for the determination of $\underline{H}(\gamma)$ from the relaxation modulus;

$$H(\gamma) = -M(n)\ m(t)\ \left.\frac{d\ \log\ m(t)}{d\ \log\ t}\right|_{t\ =\ \gamma} \tag{60}$$

where $\underline{M}(\underline{n}) = 1/\lceil(\underline{n} + 1)$, $\lceil$ is the gamma function, and $-\underline{n}$ is the slope of a double logarithmic plot of $\underline{H}(\gamma)$ _versus_ $\gamma$. The method is limited to positive $\underline{m}$ values. As a first approximation, $M(\underline{n})$ is set equal to unity and (60) becomes the first approximate relation (51) from which an estimate of $H(\gamma)$ is obtained. The negative slope of double logarithmic plot $\underline{H}(\gamma)$ _versus_ $\gamma$ is used to determine $\underline{n}$. Values of $\underline{M}(\underline{n})$ are tabulated for values of $\underline{n}$, (7), (18), and Equation (60) is corrected accordingly.

Two formulas are required to obtain $\underline{H}(\gamma)$ for the real component of the modulus depending on whether $\underline{n}$ is greater or less than unity. Usually, $\underline{n} \langle 1$, so that,

$$H(\gamma) = A\ m'(\omega)\left.\frac{d\ \log\ m'(\omega)}{d\ \log\ \omega}\right|_{\frac{1}{\omega}\ =\ \gamma,} \tag{61}$$

where

$$A = (2-n)/2\lceil(2-n/2)\lceil(1+n/2).$$

When $1 < n < 2$, the appropirate formula is

$$H(\tau) = A'm'(\omega)(2-d \log m'/d \log \omega) \Big|_{\frac{1}{\omega} = \tau} \qquad (62)$$

where

$$A' = m/2\,\Gamma(1+m/2)\,\Gamma(2-m/2).$$

As a first approximation A' is set equal to unity and a procedure similar to that already outlined is used to obtain $\underline{H}(\tau)$. The relaxation spectrum is determined from the imaginary component of the modulus by,

$$H(\tau) = B\ m''(\omega)(1- \Big| d \log m''(\omega)/d \log \omega \Big| ) \quad \Big|_{\frac{1}{\omega} = \tau} \qquad (63)$$

with

$$B = (1 + |n|)2\,\Gamma(3/2 - |n|/2)\,\Gamma(3/2 + |n|/2).$$

Retardation spectra may also be determined by the present method. Stern (20) has shown that

$$L(\tau) = M(-n)[k(t) - t/\eta]\ d \log [k(t) - t/\eta]/d \log t \Big|_{t = \tau} \qquad (64)$$

where $+\underline{n}$ is the slope of a double logarithmic plot of L versus $\tau$, and $\underline{M}(-n)$ is the same as before. This method cannot be used if creep experiments have not been carried long enough to determine $\eta$ reliably. When the real portion of the loss modulus is used,

$$L(\tau) = -A\ k'(\omega)\ d \log k'(\omega)/d \log \omega \Big|_{\frac{1}{\omega} = \tau} \qquad (65)$$

when $\underline{n} \langle 1$.    When $\underline{n} \rangle 1$ one must use,

$$L(\mathcal{T}) = A'k'(\omega) \; (2 + d \log k'(\omega)/d \log \omega) \qquad (66)$$

$$\frac{1}{\omega} =$$

with $\underline{A}'$ and $\underline{A}$ the same as before. If the imaginary compliance is used, then

$$L(\mathcal{T}) = Bk''(\omega) \; (1 - \left| d \log k''(\omega)/d \log \omega \right|) \Big|_{\frac{1}{\omega} = \mathcal{T}} \qquad (67)$$

with $\underline{B}$ as given earlier.

The method of Ferry and Williams is convenient since it involves simple graphical manipulation of logarithmic curves of modulus and compliance as a function of log time or log frequency. Since such curves must be constructed anyway in order to display experimental results, no large amount of extra work is required.

## Method of Roesler

The method of Roesler (12) is more involved than any of the preceding methods but is also potentially the most accurate. It is assumed that $\underline{m}'(\omega)$ and $\underline{m}''(\omega)$ are given as a function of $\underline{\ln}\omega$, Fig. 17. A domain $\underline{L}$ extending from 0 to $\pi$ is selected so as to include the range of $\underline{m}'(\omega)$ and $\underline{m}''(\omega)$. A variable $\underline{x}$ is chosen so that it is linearly related to $\underline{\ln}\omega$ and such that $0 \langle x \langle \pi$. The quantities $\underline{m}'(\omega)$ and $m''(\omega)$ are now expressed in terms of Fourier series in $x$, that is,

$$m'(x) = \sum_{0}^{n} c_k \cos kx \qquad (68)$$

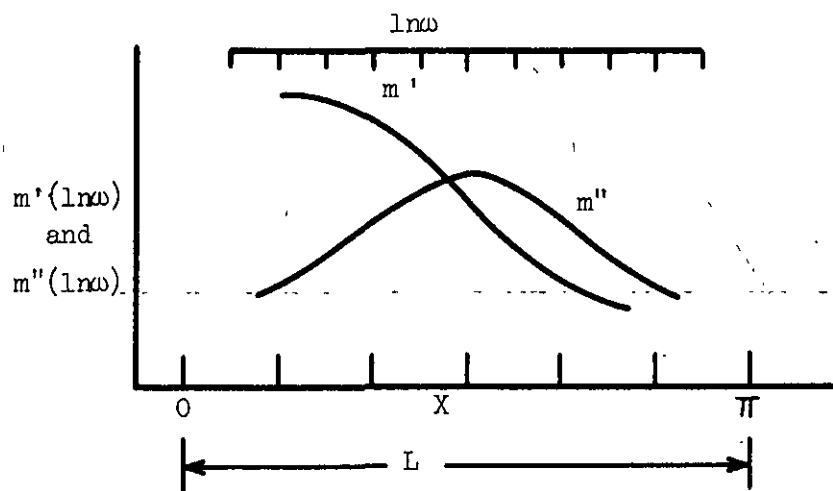and

$$m''(\omega) = \sum_{1}^{n} a_k \sin kx. \qquad (69)$$

Figure 17.  Method of Roesler Applied to the Components
of the Complex Modulus

The relaxation spectrum is then given by

$$H(x) = \sum^{n} b_k \sin kx \tag{70}$$

where the $b_k$ are related to both $a_k$ and $c_k$ by

$$b_k = \frac{2a_k}{\pi} \cosh(\frac{k\pi^2}{2L}) = \frac{2c_k}{\pi} \sinh(\frac{k\pi^2}{2L}) \tag{71}$$

and

$$a_k = c_k \tanh(\frac{k\pi^2}{2L}). \tag{72}$$

The determination of relaxation spectra from a stress relaxation experiment is considerably more complicated and will be described only briefly. The modulus $m(\ln \gamma)$ is given as a function of the variable $(\ln t)$ such that it lies within a domain $2L$, Fig. 18. A linear function $\psi(\ln \gamma)$ is defined such that the difference

$$m(\ln \gamma) - \psi(\ln \gamma) = M^*(\ln \gamma) \tag{73}$$

vanishes for those values of $\ln \gamma$ which correspond to $x = -\pi$ and $x = \pi$, Fig. 18. The function $M^*(x)$ is then fitted to the mixed Fourier series,

$$M^*(x) = \sum_{0}^{n} A_k^* \cos kx + \sum_{1}^{n} \frac{\pi}{L} k B_k^* \cos kx. \tag{74}$$

The relaxation spectrum is given by

$$H^*(x) = \sum_{1}^{n} P_k \cos kx + \sum_{1}^{n} R_k \sin kx \tag{75}$$

with

$$P_k = \frac{k\pi}{L^2} \frac{A_k^* \beta_k - B_k^* \beta_k}{\alpha_k^2 + \beta_k^2} \tag{76}$$

and

$$R_k = \frac{k\pi}{L^2} \frac{A_k^* k + B_k^* \beta_k}{\alpha_k^2 + \beta_k^2}. \tag{77}$$
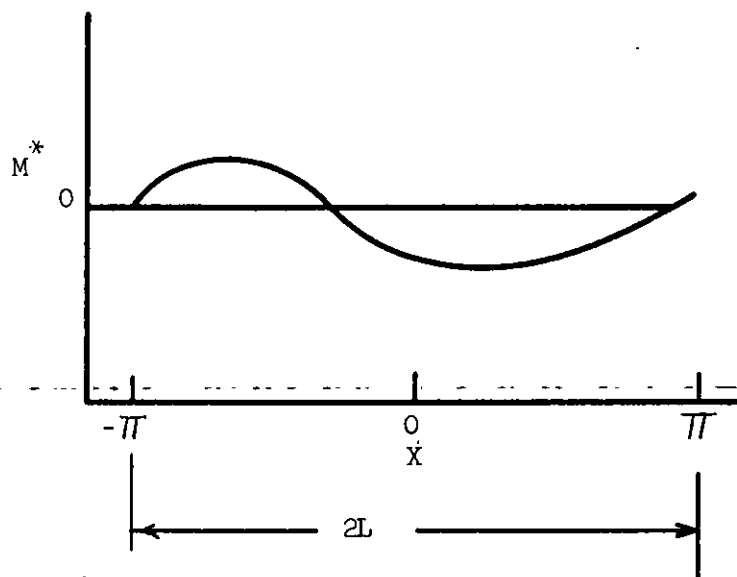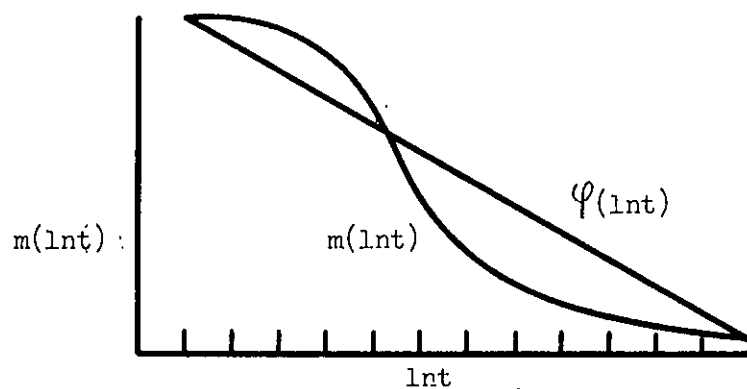
Figure 18.  Method of Roesler Applied to the Relaxation
Modulus

The coefficients $\alpha_k$ and $\beta_k$ are determined by numerical integration and are

tabulated (12) for $\underline{k}$ = 0 to 16 and depend on the value of $\underline{L}$ chosen. The tabu-

lated values are given for $\underline{L}$ = 12.8 units of $\underline{\ln} \, \gamma$, corresponding to approximately

11 decades in log $\underline{t}$. The correct relaxation spectrum is obtained by adding the

constant,

$$- \frac{d \, \varphi}{d \, \gamma} = \frac{m(-\pi) - m(\pi)}{2L} \, , \qquad (78)$$

to (75).

## Discrete Relaxation Times

A method for obtaining discrete relaxation times is described by

Tobolsky and Murakami(13). The results of a stress relaxation experiment are

expressed in terms of a discrete distribution,

$$m(t) = m_a \, \exp - t/\gamma_a + \ldots + m_{n-1} \, \exp - t/\gamma_{n-1} + m_n \, \exp - t/\gamma_n \, . \qquad (79)$$

A plot of log $\underline{m}(t)$ versus $\underline{t}$ should approach a straight line for $\underline{t} \rangle \gamma_n$ providing

a resolvable maximum relaxation time exists. The straight line will have a

slope of $-2.303/\gamma_n$ and an intercept of log $\underline{m}_n$. Equation (79) is now

rewritten in the form,

$$m(t) - m_n \, \exp - t/\gamma_n = m_a \, \exp - t/\gamma_a + \cdots + m_{n-1} \, \exp - t/\gamma_{n-1} \, . \qquad (80)$$

A plot of log $m(t) - m_n \, \exp(-t/\gamma_n)$ versus $\underline{t}$ should approach a straight line

for $\underline{t} \rangle \gamma_{n-1}$ providing a discrete relaxation time $\gamma_{n-1}$ exists and is reasonably

separated in time from $\gamma_n$ and $\gamma_{n-2}$. This process can be repeated as far as

is warranted to resolve additional relaxation times. In practice this method

when applied to monodisperse polystyrene yielded discrete relaxation times $\gamma_n$

and $\gamma_{n-1}$. The isolation of additional relaxation times might also be of significance. The ability to isolate relaxation time depends on the accuracy of long time low modulus data. This, of course, confines the measurements to the rubbery flow region for high molecular weight polystyrene. When the method is applied to polydisperse samples, relaxation times $\gamma_n$ and $\gamma_{n-1}$ are probably meaningful but additional relaxation times are probably artifacts.

The dynamic analogue has not been discussed in the literature. We have been able to devise a procedure for obtaining discrete relaxation times from the complex modulus and present it here since it differs in some respects from the case of stress relaxation. The real and imaginary components of the complex modulus are given in terms of the series,

$$m'(\omega) = \frac{m_a \omega^2 \gamma_a^2}{1+\omega^2 \gamma_a^2} + \ldots + \frac{m_{n-1}\omega^2 \gamma_{n-1}^2}{1+\omega^2 \gamma_{n-1}^2} + \frac{m_n \omega^2 \gamma_n^2}{1+\omega^2 \gamma_n^2} \tag{81}$$

and

$$m''(\omega) = \frac{m_a \omega \gamma_a}{1+\omega^2 \gamma_a^2} + \ldots + \frac{m_{n-1}\omega \gamma_{n-1}}{1+\omega^2 \gamma_{n-1}^2} + \frac{m_n \omega \gamma_n}{1+\omega^2 \gamma_n^2} \;. \tag{82}$$

If the relaxation times are sufficiently separated, so that $\gamma_n \gg \gamma_{n-1} \gg \gamma_{n-2}$, then at low frequencies when $\omega \ll 1/\gamma_n$

$$\frac{m'(\omega)}{m''(\omega)} = \omega \gamma_n = \frac{1}{\tan \delta} \;. \tag{83}$$

The relaxation time, $\gamma_n$, is to be determined from the slope of a plot of $\underline{m}'/\underline{m}''$ versus $\omega$. At low frequencies, (81) and (82) become, respectively

$$m'(\omega) = m_n \omega^2 \tau_n^2 \tag{84}$$

and

$$m''(\omega) = m_n \omega \tau_n \tag{85}$$

A plot of $\underline{m}'$ _versus_ $\omega^2$ yields a slope of $m_n \tau_n^2$ and a plot of $\underline{m}'$ _versus_ $\omega$ yields a slope $m_n \tau_n$. The value of $m_n$ can be determined from either of these slopes. An alternate and possibly better procedure is to plot $\underline{m}'$ _versus_ $\omega^2 \tau_n^2 / (1 + \omega^2 \tau_n^2)$ and $\underline{m}''$ _versus_ $\omega \tau_n / (1 + \omega^2 \tau_n^2)$. In each case the slope will yield $\underline{m}_n$ directly. Additional relaxation times may be determined as in the case of stress relaxation. The reader should bear in mind that the method has not been tested on experimental data. A critical discussion of the procedure is given by Grossman (21) where the use and limitations of the method are analyzed.

LITERATURE CITED

1. Leaderman, H., Trans. Soc. Rheology 1:213-22(1957).

2. Maxwell, J. C., Phil. Trans. Roy. Soc. (London), 157:52(1867).

3. Kelvin, Encyclopaedia Brittanica(1875).

4. Voigt, W., Abh. K. Ges. Wiss. Göttingen 36, (1890).

5. Boltzmann, L., Sitzber, Kgl. Akad. Wiss. Wien., Math.-Naturw. Classe 70: 275(1874) = Pogg. Ann. Physik 7:624(1876).

6. Gross, B. Mathematical structure of the theories of viscoelasticity, Hermann et Cie, Paris, 1953.

7. Ferry, J. D. Viscoelastic properties of polymers, Wiley, New York (1961).

8. Leaderman, H. Creep of filamentous materials and other high polymers, The Textile Foundation, Washington, 1943.

9. Becker R., Zeits. Physik., 33:185(1925).

10. Andrews, R. D., Ind. and Engr. Chem. 44:707(1952).

11. Ferry, J. D., and Williams, M. L., J. Colloid Sci. 7:347(1952).

12. Roesler, F. C., Proc. Phys. Soc., B68:89(1955).

13. Tobolsky, A. V., and Murakami, K., J. Poly. Sci. 40:443(1959).

14. Schwarzl, F., and Staverman, A. J., Appl. Sci. Research, A4:127(1953).

15. Okano, M., Busseiran Kenkyu 3:493(1958).

16. Fujita, H., J. Applied Phys. 29:943(1958).

17. Roesler, F. C., and Twyman, W. A., Proc. Phys. Soc. B68:97(1955).

18. Ninamiya, K., and Ferry, J. D., J. Colloid Sci. 14:36(1959).

19. Ferry, J. D., and Williams, M. L., J. Colloid Sci. 7:347(1952).

20. Stern, D. M. Ph.D. Thesis, University of Wisconsin. (1956).

21. Grossman, P. U. A., J. Poly Sci. 46, 257(1960).